A large-scale simulation model to assess karstic groundwater recharge over Europe and the Mediterranean

A. Hartmann[1,3], Tom Gleeson[2], Rafael Rosolem[1], Francesca Pianosi[1], Yoshihide Wada[4], Thorsten Wagener[1]

[1] Department of Civil Engineering, University of Bristol, United Kingdom

[2] Civil Engineering, McGill University, Canada

[3] Faculty of Environment and Natural Resources, University of Freiburg, Germany

[4] Department of Physical Geography, Utrecht University, The Netherlands

Correspondence to: A. Hartmann (aj.hartmann@bristol.ac.uk)

Resubmitted to Geoscientific Model Development March 2015

Abstract

Karst develops through the dissolution of carbonate rock and is a major source of groundwater contributing up to half of the total drinking water supply in some European countries. Previous approaches to model future water availability in Europe are either too-small scale or do not incorporate karst processes, i.e. preferential flow paths. This study presents the first simulations of groundwater recharge in all karst regions in Europe with a parsimonious karst hydrology model. A novel parameter confinement strategy combines *a priori* information with recharge-related observations (actual evapotranspiration and soil moisture) at locations across Europe while explicitly identifying uncertainty in the model parameters. Europe's karst regions are divided into 4 typical karst landscapes (humid, mountain, Mediterranean and desert) by cluster analysis and recharge is simulated from 2002 to 2012 for each karst landscape. Mean annual recharge ranges from negligible in deserts to

>1 m/a in humid regions. The majority of recharge rates ranges from 20%-50% of precipitation and are sensitive to sub-annual climate variability. Simulation results are consistent with independent observations of mean annual recharge and significantly better than other global hydrology models that do not consider karst processes (PCR-GLOBWB, WaterGAP). Global hydrology models systematically underestimate karst recharge implying that they over-estimate actual evapotranspiration and surface runoff. Karst water budgets and thus information to support management decisions regarding drinking water supply and flood risk are significantly improved by our model.

1 Introduction

Groundwater is the main source of water supply for billions of people in the world (Gleeson et al., 2012). Carbonate rock regions only constitute about 35% of Europe's land surface (Williams and Ford, 2006), yet contribute up to 50% of the national water supply in some European countries (COST, 1995) because of their high storage capacity and permeability (Ford and Williams, 2007). Climate conditions have a primary control on groundwater recharge (de Vries and Simmers, 2002). Climate simulations suggest that in the next 90 years Mediterranean regions will be exposed to higher temperatures and lower precipitation amounts (Christensen et al., 2007). In addition, shifts in hydrological regimes (Milly et al., 2005) and hydrological extremes (Dai, 2012; Hirabayashi et al., 2013) can be expected. To assess the impact of climate change on regional groundwater resources as groundwater depletion or deteriorations of water quality, large-scale simulation models are necessary that go beyond the typical scale of aquifer simulation models (~10-10,000 km²) Additionally, we expect the future variability of climate to be beyond that reflected in historical observations, which means that model predictions should derive credibility via more in-depth diagnostic evaluation of the consistency between the model and the underlying system and not from some calibration exercise (Wagener et al., 2010).

Currently available global hydrology models discretise the land surface in grids with a resolution down to 0.25 to 0.5 decimal degrees. Parts of the vertical fluxes are well represented, e.g. the energy balance (Ek, 2003; Miralles et al., 2011). But groundwater recharge and groundwater flow are represented simply by heuristic equations (Döll and Fiedler, 2008a) or assumptions of linearity (Wada et al., 2010, 2014). They do not explicitly simulate a dynamic water table or regional groundwater flow. Global models also assume

homogenous conditions of hydrologic and hydraulic properties in each of their grid cells, rather than variable flow paths, and they completely omit the possibility of preferential flow. This was criticized in the recent scientific discourse about the need for large-scale hyper-resolution models (Beven and Cloke, 2012; Wood et al., 2011).

The assumption of homogeneity is certainly inappropriate for karst regions. Chemical weathering of carbonate rock and other physical processes develop preferential pathways and strong subsurface heterogeneity (Bakalowicz, 2005). Flow and storage are heterogeneous ranging from very slow diffusion to rapid concentrated flow at the surface, in the soil, the unsaturated zone and the aquifer (Kiraly, 1998). A range of modeling studies have developed and applied karst specific models at individual karst systems at the catchment or aquifer scale (Doummar et al., 2012; Fleury et al., 2007; Hartmann et al., 2013b; Le Moine et al., 2008) but a lack of *a priori* information of aquifer properties and observations of groundwater dynamics have prohibited their application on larger scales (Hartmann et al., 2014a).

Compared to the limited information about the deeper subsurface there is much better information about the surface and shallow subsurface including maps of soil types and properties (FAO/IIASA/ISRIC/ISSCAS/JRCv, 2012), observations of soil moisture (International Soil Moisture Network, Dorigo et al., 2011) and of latent heat fluxes (FluxNet, Baldocchi et al., 2001), as well as river discharge (GRDC, 2004). Surface and shallow subsurface information is used for the parameterization and evaluation of the surface routines of present large-scale models. But, although these data also cover Europe's karst regions, it has not been used for the development of large-scale models to simulate karstic surface and shallow subsurface flow and storage dynamics.

The objective of this study is to develop the first large-scale simulation model for karstic groundwater recharge over Europe and the Mediterranean. Despite much broader definitions of groundwater recharge (e.g., Lerner et al., 1990), we focus on potential recharge, that is vertical percolation from the soil below the depth affected by evapotranspiration. We use a novel type of model structure that considers the sub-grid heterogeneity of karst properties using statistical distribution functions. To achieve a realistic parameterization of the model we identify typical karst landscapes by cluster analysis and by a combined use of *a priori* information about soil storage capacities and observations of recharge related fluxes and storage dynamics. Applying a parameter confinement strategy based on Monte Carlo

sampling we are able to provide large-scale simulation of annual recharge including a quantification of their uncertainty.

2 Data and Methods

Due to chemical weathering (karstification) karst systems have a strong subsurface heterogeneity of flow and storage processes (Bakalowicz, 2005) that have to be considered to produce realistic simulations (Hartmann et al., 2014a). In this study, large-scale karst recharge is estimated by a modified version of the VarKarst model (Hartmann et al., 2013a), called VarKarst-R from here, on a 0.25 x 0.25 decimal degree grid. The model has shown to be applicable at various scales and climates over Europe (Hartmann et al., 2013b). To apply the model on a large scale we developed a new parameter estimation procedure that separates the study area into four karst landscapes by cluster analysis and estimates model parameters and their uncertainty by a step-wise parameter confinement process.

2.1 The model

The VarKarst-R model simulates potential recharge, which is the water column the vertically percolated from the soil and epikarst. Hence, the previous version of the model is reduced to include only the soil and the epikarst simulation routines but still using the same statistical distribution functions that allow for variable soil depths, variable epikarst depths and variable subsurface dynamics (Figure 1). This leads to a parametrically efficient process representation. Comparisons with independently derived field data showed that these distribution functions are a good approximation of the natural heterogeneity (Hartmann et al., 2014b).

Heterogeneity of soil depths is represented by a mean soil storage capacity V_{soil} [mm] and a variability constant a [-]. The soil storage capacity $V_{S,i}$ [mm] for every compartment i is defined by:

$$V_{S,i} = V_{\max,S} \cdot \left(\frac{i}{N} \right)^a \quad (1)$$

where $V_{max,S}$ [mm] is the maximum soil storage capacity and N is the total number of model compartments. This is derived from the mean soil storage capacity V_{soil} as

$$\int_0^{i_{1/2}} V_{\max,S}\left(\frac{x}{N}\right)^a dx = \frac{\int_0^N V_{\max,S}\left(\frac{x}{N}\right)^a dx}{2}; V_{soil} = V_{\max,S}\left(\frac{i_{1/2}}{N}\right)^a$$

$$\Updownarrow \qquad . \qquad (2)$$

$$V_{\max,S} = V_{soil} \cdot 2^{\left(\frac{a}{a+1}\right)}$$

where $i_{1/2}$ is the compartment at which the soil storage capacities on the left equal the soil storage capacities on the right (Figure 1a). Preceding work (Hartmann et al., 2013a, 2013b) showed that the same distribution coefficient a can be used to derive the epikarst storage distribution $V_{E,i}$ from the mean epikarst storage capacity V_{epi} [mm] (via the maximum epikarst storage $V_{max,E}$ likewise to $V_{max,S}$ in Eq (2)):

$$V_{E,i} = V_{\max,E} \cdot \left(\frac{i}{N}\right)^a \qquad (3)$$

At each time step t, the actual evapotranspiration from each soil compartment $E_{act,i}$ is found by:

$$E_{act,i}(t) = E_{pot}(t) \cdot \frac{\min\left[V_{Soil,i}(t) + P_{eff}(t) + Q_{Surface,i}(t), V_{S,i}\right]}{V_{S,i}} \qquad (4)$$

where E_{pot} [mm] is the potential evapotranspiration derived by the Priestley-Taylor equation (Priestley and Taylor, 1972), P_{eff} [mm] is the sum of liquid precipitation and snow melt, $Q_{surface,i}$ [mm] is the surface inflow arriving from compartment i-1 (see Eq. (9)), and $V_{S,i}$ [mm] the water stored in the soil at time step t. Snow fall and snow melt are derived from daily snow water equivalent available from GLDAS-2 (Table 1). During days with snow cover we set $E_{act}(t)$=0. Flow from the soil to the epikarst $R_{Epi,i}$ [mm] is calculated by:

$$R_{Epi,i}(t) = \max\left[V_{Soil,i}(t) + P_{eff}(t) + Q_{Surface,i}(t) - E_{act,i}(t) - V_{S,i}, 0\right] \qquad (5)$$

Following an assumption of linearity (Rimmer and Hartmann, 2012), the epikarst storage coefficients $K_{E,i}$ [d] controls the epikarst outflow dynamics:

$$Q_{Epi,i}(t) = \frac{\min\left[V_{Epi,i}(t) + R_{Epi,i}(t), V_{E,i}\right]}{K_{E,i}} \cdot \Delta t \qquad (6)$$

$$K_{E,i} = K_{Epi} \cdot \left(\frac{N - i + 1}{N}\right)^a \qquad (7)$$

where $V_{E,i}$ [mm] is the water stored in compartment *i* of the epikarst at time step *t*. Again, the same distribution coefficient *a* is applied to derive $K_{E,i}$ from the mean epikarst storage coefficient K_{Epi}. The latter is obtained from the mean epikarst storage coefficient K_{epi} using:

$$N \cdot K_{mean,E} = \int_0^N K_{\max,E}\left(\frac{x}{N}\right)^a dx$$
$$\Updownarrow \qquad (8)$$
$$K_{\max,E} = K_{epi} \cdot (a+1)$$

When infiltration exceeds the soil and epikarst storage capacities, surface flow to the next model compartment $Q_{Surf,i+1}$ [mm] initiates:

$$Q_{Surf,i+1}(t) = \max\left[V_{Epi,i}(t) + R_{Epi,i}(t) - V_{E,i}, 0\right] \qquad (9)$$

To summarize, the model is completely defined by the four parameters *a*, K_{epi}, V_{soil}, and V_{epi} (Table 2).

2.2 Data availability

Forcing for the VarKarst-R model is derived through the Global Land Data Assimilation System (GLDAS-2) that assimilates satellite- and ground-based observational data products to obtain optimal fields of land surface states and fluxes (Rodell et al., 2004; Rui and Beaudoing, 2013). While precipitation, temperature and net radiation are mainly merged from satellite and gauge observations, snow water equivalent is derived using data assimilation as well as the snow water equivalent simulations of the NOAH land surface model v3.3 (Ek, 2003) driven by GLDAS-2 forcing. Europe's and the Mediterranean's carbonate rock areas are derived from a global map (vector data) of carbonate rock (Williams and Ford, 2006). Each cell of the 0.25 decimal degree simulation grid intersecting a carbonate rock region was considered a karst region. The model was calibrated and evaluated with observations of actual evapotranspiration from the FLUXNET (Baldocchi et al., 2001) and with soil water content data from the International Soil Moisture Network ISMN (Dorigo et al., 2011). Only stations within carbonate rock regions and with ≥12 months of available data were used (Figure 2). Months with <25 days of observations were discarded. In addition, months with ≥50% mismatch in their energy closure were discard from the FLUXNET data set (similar to Miralles et al., 2011).

2.3 Parameter estimation

A lack of *a priori* information and observations of discharge and groundwater levels that can be used for calibration are the primary reasons why karst models have not been applied on larger scales yet (Hartmann et al., 2014a). The parameter assessment strategy we present in the following is meant to overcome this problem by using a combination of *a priori* information and recharge-related variables. We define typical karst landscapes over Europe and the Mediterranean and apply this combined information to a large initial sample of possible model parameter sets. In a step-wise process we then discard all parameter sets that produce simulations inconsistent with our *a priori* information and our recharge-related observations.

2.3.1 Definition of typical karst landscapes

Our definition of typical karst landscapes is based on the well-known the hydrologic landscape concept (Winter, 2001), which describes hydrological landscapes based on their geology, relief and climate. Constraining ourselves to karst regions that mainly develop on carbonate rock we assume that differences among the karst landscapes are due to differences in relief and climate, and the consequent processes of landscape evolution including the weathering of carbonate rock (karstification). The carbonate rock regions in Europe and the Mediterranean are divided into typical landscapes using simple descriptors of relief (range of altitude RA) and climate (aridity index AI and mean annual number of days with snow cover DS) within each of 0.25 decimal degree grid cells and a standard cluster analysis scheme (k-means method). We test the quality of clustering for 2 to 20 clusters by calculating the sums of squared internal distances to the cluster means. The so-called “elbow method” identifies the point where adding additional clusters only leads to a marginal reduction in the internal distance metric, i.e. the percentage of variance explained by adding more clusters would not increase significantly (Seber, 2009).

2.3.2 Model parameters for each karst landscape

We initially sample 25,000 possible model parameter sets from independent uniform distributions using parameter ranges derived from previous catchment scale applications of the VarKarst-R model over Europe and the Mediterranean (Table 2). We use *a priori* information and recharge-related observations to assess parameter performance for each karst landscape. *A priori* information consists of spatially distributed information about mean soil

storage capacities as provided by several preceding mapping and modelling studies (Ek, 2003; FAO/IIASA/ISRIC/ISSCAS/JRCv, 2012; Miralles et al., 2011). Recharge-related variables are (1) soil moisture observations and (2) observations of actual evaporation at various locations over the modelling domain (Table 1, Figure 2). Soil moisture is related to recharge because it indicates the start and duration of saturation of the soil during which diffuse and preferential recharge can take place. Actual evaporation is related to recharge because usually no surface runoff occurs in karst regions due to the high infiltration capacities (Jeannin and Grasso, 1997). The difference of monthly precipitation and actual evaporation is therefore a valid proxy for groundwater recharge at a monthly time scale or above. The new parameter confinement strategy is applied to each of the karst landscapes in 3 steps:

1. Bias rule: retain only the parameter sets that produce a bias between observed and simulated actual evaporation lower than 75% at all FLUXNET locations within the chosen karst landscape:

$$\min_i\left(bias_i\right)=\min_i\left(\frac{\mu_{sim,i}-\mu_{obs,i}}{\mu_{obs,i}}\right)\overset{!}{<}75\% \tag{10}$$

   Where $m_{sim,i}$ and $m_{obs,i}$ are the sum of simulated and observed actual evapotranspiration at location *i*, respectively. The value 75% was found by trial-and-error, which reduced the initial sample to a reasonable number. The bias rule was not applied on the soil moisture since porosities of the soil matrix were not available prohibiting a comparison of simulated and observed soil water contents.

2. Correlation rule: retain only the parameter sets that produce a positive coefficient of (Pearson) correlation between observations and simulations of both actual evaporation and soil moisture, at all locations:

$$\left(\min_i\left[corr(AET_{sim,i},AET_{obs,i}\right]\wedge\min_j\left[corr(\theta_{sim,j},\theta_{obs,j}\right]\right)\overset{!}{>}0 \tag{11}$$

   where $AET_{sim,j}$ and $AET_{obs,j}$, and $\theta_{sim,j}$ and $\theta_{obs,j}$ are the monthly means of simulated and observed actual evapotranspiration, and soil water content at locations *i/j*, respectively.

3. Application of *a priori* information: retain only parameter sets in which V_{soil} falls within the feasible ranges that can be derived from *a priori* information about the maximum soil storage capacity in different karst landscapes (Ek, 2003;

FAO/IIASA/ISRIC/ISSCAS/JRCv, 2012; Miralles et al., 2011). Less than usual we add the *a priori* information at the last step to evaluate if the *posterior* distributions of V_{soil} already adapt to the ranges defined in this confinement step. If they do not we would conclude that the recharge related information applied in confinement steps 1 and 2 is biased. If they do, we have indication that the data applied in all 3 steps is complementary.

Each step reduces the initial parameter sample differently for each of the karst landscapes. The *posterior* parameter distributions within the confined samples should be different among the karst landscapes if the karst landscapes are properly defined. The rather weak thresholds in step 1 and 2 were chosen to take into account the uncertainties resulting from the differences in scales of observations (point) and simulations (grid cell), and from the indirect observation of recharge (actual evaporation and soil moisture as recharge related variables).

2.4 Recharge simulations over Europe and the Mediterranean

Recharge is simulated over the carbonate regions of Europe and the Mediterranean from 2002/03 to 2011/12 using the confined parameter samples for each of the identified karst landscapes and the available forcings (Table 1). The mean and standard deviation of simulated recharge for each grid cell and time step is calculated by uniform discrete sampling of a representative subset of 250 parameter sets from each of the confined parameters sets which we regarded to be large enough to provide a reliable measure of spread.

2.5 Model evaluation

To assess the realism of simulated groundwater recharge we compare simulated with observed mean annual recharge volumes derived independently from karst studies over Europe and the Mediterranean (Table 3). In addition, we compare our results to the simulated mean annual recharge volumes of two well-established global simulation models: PCR-GLOBWB (Wada et al., 2010, 2014) and WaterGAP (Döll and Fiedler, 2008a; Döll et al., 2003).

We furthermore apply a global sensitivity analysis strategy, called Regional Sensitivity Analysis (Spear and Hornberger, 1980), to evaluate the importance of the 4 model parameters at different simulation time scales ranging from 1 month up to 10 years. This analysis shows (1) which simulated process and characteristics are dominant at a given time scale and (2)

256 which parameters will need more careful calibration when the model will be used in future
257 studies. We use the same sample of 25,000 parameter sets that was created for the parameter
258 estimation strategy (subsection 2.3.2) and assess the sensitivity of 4 model outputs
259 representative of different time scales: coefficient of variation (CV) of simulated monthly
260 recharge volumes (monthly), CV of simulated 3-monthly recharge volumes (seasonal), CV of
261 annual recharge volumes (annual), and total recharge over the entire 10-year simulation
262 period (decadal). We do not consider temporal resolution less than a month given the
263 assumption that the difference of precipitation and actual evapotranspiration can be a proxy
264 for groundwater recharge, and due to uncertainties related to differences in simulation (grid
265 cell) and observation (point).

266 For each of the identified karst landscapes we choose the 10 locations that are closest to their
267 cluster means (Euclidean distances to relief and climate descriptors; subsection 2.3.1) as
268 representative locations. In the regional sensitivity analysis approach, we split the parameter
269 sets into two groups, those that produce simulations above the simulated median of one of the
270 4 model outputs and those that produce simulations below. We then calculate the maximum
271 distance D(x) between marginal cumulative distribution functions (CDFs) produced by these
272 two distributions for each of the parameters – a large distance D(x) suggests that the
273 parameter is important for simulating this particular output (Figure 3).

274 # 3 Results

275 ## 3.1 Parameter assessment

276 ### 3.1.1 Definition of typical karst landscapes

277 Cluster analysis resulted in four clusters, which are generally spatially contiguous (Figure 4)
278 and have quantitatively distinct cluster means (Table 4). We can attribute particular
279 characteristics to each cluster using the mean values of the clustering descriptors (Table 4):
280 (1) Humid hills and plains (HUM) are characterised by an aridity index <1, a significant
281 number of days with snow cover and low elevation differences. (2) High range mountains
282 (MTN) have an aridity index of ~1, they also have a significant number of days with snow
283 cover and they show very large topographic elevation differences. (3) Mediterranean medium
284 range mountains (MED) show a high aridity index, only few days with snow cover and high
285 elevation differences. (4) Desert hills and plains (DES) are described by similar altitude
286 ranges as the humid hills and plains but they have a high aridity indices and almost no days

with snow cover. The karst landscapes order from North (HUM) to South (DES) based on increasing temperatures and decreasing precipitation amounts. While HUM and DES appear to be separated clearly, MTN and MED mix in some regions, for instance Greece and Turkey where mountainous regions are in close proximity to the coast.

3.1.2 Model parameter estimates for each karst landscape

The three steps of the new parameter confinement strategy resulted in a significant reduction of the initial sample of 25,000 parameter sets (Figure 5). Each step has a different impact on the reduction among the identified landscapes. For the humid karst landscapes, the correlation rule appears to have the strongest impact while for the mountain and Mediterranean landscapes the bias rule results in the strongest reduction. For the desert landscape only step 3, i.e. application of *a priori* information, reduces the initial sample because no data was available to apply steps 1 and 2. Considering the parameter ranges for each landscape after the application of the confinement strategy (Table 5), we only achieved a confinement of the distribution parameter a, the soil storage capacity V_{soil}, and slight confinement of the epikarst storage coefficient K_{epi}.

The impact of the three confinement steps becomes more obvious when considering their *posterior* distributions (Figure 6). The distributions of parameters a, K_{epi} and V_{soil} evolve significantly away from their initial uniform distributions along the confinement steps. In general, changes of the *posterior* distributions of each landscape's parameter samples are in accordance with the reductions of their number (Figure 5), though changes are pronounced differently among the parameters. While a and V_{soil} change strongly for HUM, MTN and MED, V_{epi} maintains a uniform distribution across all steps. K_{epi} also exhibits strong changes for HUM but they are less pronounced for MTN and MED. The *posterior* distributions of the DES landscape do not change except for step 3 due to the lack of information to apply confinement steps 1 and 2. Step 3 results in a tailoring of the distribution of V_{soil} for all landscapes. For HUM, MTN and MED it can be seen that confinement steps 1 and 2 already pushed the parameter distributions towards their final shape, meaning that the changes in parameter distributions induced by the comparison with observations are consistent with the *a priori* information about the physical characteristics of the karst.

3.2 Recharge simulations over Europe and the Mediterranean

The parameter confinement strategy allows us to apply VarKarst-R over all of Europe and the Mediterranean, and to obtain recharge simulations for the hydrological years 2002/03-2011/12. Thanks to the 250 parameter sets that we samples from the *posterior* parameter distributions we can include an estimate of uncertainty for each grid cell (Figure 7). Mean annual recharge ranges from almost 0 to >1000 mm/a with the highest volumes found in Northern UK, the Alps and former Yugoslavia. The lowest values are found in the desert regions of Northern Africa. The vast majority of recharge rates ranges from 20%-50% of precipitation. Considering the simulations individually for each karst landscape reveals that the mountain landscapes produce the largest recharge volumes followed by the humid and Mediterranean landscapes (Figure 8a). The desert landscapes produce the lowest recharge volumes. However, the recharge rates reveal that on average the Mediterranean landscapes show the largest recharge rates, followed by the highly variable mountains (Figure 8c). Humid and deserts landscapes exhibit lower recharge rates. Uncertainties, expressed by the standard deviation of the 250 simulations for each grid cell, are rather low, seldom exceeding 35 mm/a (Figure 8b). However, expressed as coefficients of variation, most of them range from 5%-25% for the humid, mountain and Mediterranean landscapes but for the desert landscape they can reach up to 50% of the mean annual recharge (Figure 8d).

3.3 Model evaluation

We compare the simulated recharge volumes of our model with recharge volumes assessed from independent and published karst studies over Europe and the Mediterranean (Figure 9a). Even though there is a considerable spread across the simulations their bulk plots well around the 1:1 line achieving an average deviation of only -22 mm/a (Table 6). Considering the individual karst landscapes there is an over-estimation of recharge for the humid landscapes and an under-estimation for the mountain landscapes. The best results are achieved for the Mediterranean landscapes with only slight under-estimation (Figure 9a). When we compare the same observations to the simulated recharge volumes of the PCR-GLOBWB (Figure 9b) and WaterGAP models (Figure 9c) we find a strong tendency of under-estimation that is strongest for the mountain and Mediterranean landscapes but still significant for the humid landscapes (Table 6). For the humid landscapes absolute deviations are similar among the three models.

In addition to comparing simulated and observed annual averages, sensitivity analysis on the model output gives us insight in the realism of the model and the importance of individual model parameters at different time scales (Figure 10). Our results show that parameters *a* and V_{soil} have the overall strongest influence on the simulated recharge from a monthly to a 10-year time scale but their influence decreases toward shorter time scales. Simultaneously the epikarst parameter K_{epi} gains more importance. This behaviour is most pronounced for the Mediterranean and desert landscapes. The same is true for V_{epi}, but its overall importance remains much lower, which was also found in the parameter confinement strategy (Figure 6).

4 Discussion

4.1 Reliability of parameter estimation

4.1.1 Identification of karst landscapes

The identification of different karst landscapes is a crucial step within our new parameter estimation strategy. The four karst landscapes we identified depend mostly on the choice of climatic and topographic descriptors (Table 4) and the selected number of clusters. Even though neglecting several factors as depositional environments, fracturing by tectonic processes or regional variations in rain acidity our choice of descriptors is well justified from our understanding of dominant hydrologic process controls as formalized in the hydrologic landscape concept (Winter, 2001) and applied similarly at many other studies (Leibowitz et al., 2014; Sawicz et al., 2011; Wigington et al., 2013). The appropriate choice of clusters for the k-means method is less unambiguous (Ketchen and Shook, 1996). The change in number of clusters when the sum of squared distances to our cluster centres only reduces marginally was not clearly definable (Figure A 1). However, choosing only 3 clusters instead of 4 would have resulted in unrealistic spatial distribution of clusters. The attribution of Northern African regions with Northern Europe to the same cluster occurred because of their similarity of altitude ranges (Table 4). On the other hand, a selection of 5 clusters would have resulted in a cluster with properties just between the MTN and the MED clusters and, because of a much stronger scattering, weaker spatial distinction between them. With 4 clusters our karst landscapes are similar to the Koeppen Geiger climate regions (Kottek et al., 2006), in particular the Oceanic Climate (HUM), the Hot and Warm summer Mediterranean Climate (MED), and the Hot Desert Climates (DES). We see deviations when comparing the Polar and

Alpine Climate regions of Koeppen-Geiger with our High Range Mountain karst landscape though, since our landscapes are also defined by their elevation ranges.

The borders of these hydrologic landscapes are also uncertain. Natural systems usually do not have straight borders that fall on a grid as assumed by this analysis. Typical transitions between landscape types are continuous and hence transitions from a parameter set representing one landscape to another parameter set of another cluster should be graded, as well. This will be discussed in the following subsection.

4.1.2 Confinement of parameters

How the 3 steps of the parameter confinement strategy reduce the initial sample shows which type of data provides the most relevant information for each of the karst landscapes. While the timing of actual evapotranspiration and soil saturation that is expressed by the correlation rule appears to be most relevant for the humid landscapes, the bias rule, which represents the volumes of monthly evapotranspiration is more relevant for the mountain and Mediterranean landscapes. Swapping the order of the correlation rule and the bias rule would provide the same results for HUM and MTN. But for MED the alternative order increases the importance of timing expressed by the correlation rule indicating the similar importance of both confinement steps.

The thresholds we set in confinement step 1 and 2 are not very strict, and the ranges of soil storage capacity we used as *a priori* information in step 3 are quite large This compensates for the fact that (1) only recharge-related variables are available rather than direct recharge observations, (2) these variables are not available at the simulation scale (0.25° grid) but at a point-scale, and (3) the transition between the landscapes is more continuous than discrete. Despite these rather weak constraints, the initial parameter sample of 25,000 reduces to a quite low numbers between 679 (HUM) and 2,731 (MED). All *posterior* parameters overlap except for the soil storage capacities that are tailored by the *a priori* information (confinement step 3). Hence, a little number of parameter sets for one landscape is also acceptable for some of the other landscape and therefore taking into account the continuous transition between them.

All model parameters, except for V_{epi}, show different shapes in their cumulative distribution functions across the karst landscapes. The desert landscape parameters only differ from the initial sample for the V_{soil} parameter due to the lack of information to apply confinement steps

1 and 2. The distribution parameter *a* is found at the lower values of its feasible range for the humid and mountain landscapes indicating a significant contribution of preferential recharge. Since altitude ranges are rather low for HUM this may be attributed to a significant epikarst development (Perrin et al., 2003; Williams, 1983). For MTN a mixture of epikarst development and topography driven interflow at the mountain hill slopes and valleys can be expected to control the dynamics of karstic recharge (Scanlon et al., 2002; Tague and Grant, 2009). At the Mediterranean landscapes the *a* parameter adapts to ranges that are rather found at the higher values of its initial range indicating that there is a stronger differentiation between diffuse and concentrated recharge. This may be due to the generally thinner soils (Table 5) that limit the availability of CO_2 for karst evolution (Ford and Williams, 2007). Instead, local surface runoff channels the water to the next enlarged fissure or crack to reach the subsurface as concentrated recharge (Lange et al., 2003). The epikarst storage coefficient K_{epi} for HUM and MED is at lower values of the initial range indicating realistic mean residence times of days to weeks (Aquilina et al., 2006; Hartmann et al., 2013a). The MTN landscapes show larger K_{epi} values indicating slower epikarst dynamics most probably due to the reasons mentioned above. The application of *a priori* information in confinement step 3 automatically tailors the values of V_{soil} to ranges that we assume to be realistic. The fact that confinement steps 1 and 2 already push the shape of their *posteriors* towards the *a priori* ranges corroborates that assumption.

The little changes that occur to the initial distributions of the DES parameter sets elaborate the flexibility of our parameter assessment strategy. The *posterior* distribution evolves only where information is available (for this landscape on V_{soil}). This is also evident in the behaviour of parameter V_{epi}. The available information is just not precise enough to achieve identification beyond its *a priori* ranges. For parameter *a* in HUM, MTN and MED, a lot of information is derived from the available data and its *posteriors* differ strongly from its initial distribution, while there is less information to determine K_{epi}. This explicit handling of uncertainties in the parameter identification process allows us to provide recharge simulations over Europe's karst regions with uncertainty estimates that represent confidence for each of the identified karst landscapes.

4.2 Simulation of karst recharge over Europe and the Mediterranean

4.2.1 Realism of spatial patterns

Simulated mean annual recharge amounts for the period 2002/03-2011/12 show a wide range of values, from 0 >1000 mm/a (Figure 7). Total water availability (mean annual precipitation) appears to be the main driver for its spatial pattern in many regions, for instance at former Yugoslavia or Northern UK. This is consistent with findings of other studies (Hartmann et al., 2014c; Samuels et al., 2010). When we normalize the recharge rates by the observed precipitation amounts we find that water availability is not the only control on mean annual recharge volumes. A strong relation of evapotranspiration and karst characteristics and processes was shown in many studies and is also found here (Heilman et al., 2014; Jukic and Denic-Jukic, 2008). Potential evaporation is generally increasing from North to South and has an important impact on recharge rates as well; for instance on the Arabian Peninsula or in the Alps.

Mountain ranges are considered to be the water towers of the world (Viviroli et al., 2007). Here the MTN landscapes also show the largest recharge volumes due to the large precipitation volumes they receive, though with a considerable spread in our study. HUM and MED landscapes behave similarly with significantly less recharge than MTN. Not surprisingly there is not much recharge in the desert landscapes at all. But the differences among the clusters shift when considering recharge rates. Due to their thin soils, and therefore low soil storage for evaporation (Table 5), the DES karst landscapes transfer up to 45% of the little precipitation they receive into recharge. The MED landscapes show similarly high recharge rates. Though since their soils are generally thicker than the DES soils the typical seasonal and convective rainfall patterns of the Mediterranean climate (Goldreich, 2003; Lionello, 2012) might have an important impact, too.

Even though there is still considerable spread in our confined parameter sets, the uncertainty in simulated mean annual recharge volumes is quite low. The uncertainties that follow the limited information contained in the observations are revealed more clearly when we relate the standard deviation of simulated recharge to its mean volumes with the coefficient of variation. The uncertainty for the DES landscape is the largest among the clusters because *a priori* information is only available for V_{soil}. The uncertainty reduces for the MED and MTN landscapes. The low uncertainties for the coefficient of variation of our recharge simulations

for the HUM landscape indicate that the available data contained significant information for confining the model parameter ranges.

4.2.2 Relevance of different recharge processes to simulation time scales

The mean annual water balance of a hydrological system is dominated by the separation of precipitation into actual evapotranspiration and discharge (Budyko and Miller, 1974; Sivapalan et al., 2011). Actual evapotranspiration is controlled by the soil storage capacity V_{soil} and the distribution coefficient a within the VarKarst-R model. Regional sensitivity analysis shows that both of them are most sensitive for the 10-year and annual time scale (Figure 10). Both parameters loose some impact at higher temporal resolutions (seasonal or monthly time scale) in favour of the parameters that control the dynamics of the epikarst. This behaviour is consistent with evidence from field and other modelling studies that showed that the epikarst can be considered as a temporary storage and distribution system for karstic recharge (Hartmann et al., 2012; Williams, 1983) – potentially storing water for several days to weeks (Aquilina et al., 2006; Hartmann et al., 2013a). Parameter V_{epi} does not show much sensitivity across all landscapes as suggested by the *posterior* distributions of the confinement strategy. First of all, this finding indicates that the data we used for our confinement strategy do not bias the general model behaviour. It also shows that for the epikarst storage and flow dynamics K_{epi} is much more important when simulating at monthly or seasonal resolution.

Furthermore, the results of the regional sensitivity analysis show which parameters are most important at a given time scale. Depending on the purpose a new study may start with the initial ranges of the model parameters or it might continue with the confined parameter ranges that we found here. The latter would result in slightly different sensitivities (Figure A 2). For both cases, the epikarst parameters will require more attention when applying the VarKarst-R model for simulations at seasonal or monthly time scales. When working at a smaller spatial scale, combined analysis of spring discharge and its hydrochemistry may provide such additional information (Lee and Krothe, 2001; Mudarra and Andreo, 2011). When working at a time scale of >1 year the variability constant a and the soil storage capacity V_{soil} require most attention if one starts from the initial ranges. The distribution parameter is most important when using the confined ranges. Again, spring discharge analysis may help to understand the degree of karstification (Kiraly, 2003) and the distribution of concentrated and diffuse recharge mechanisms that are controlled by a. In addition, more precise digital elevation models or soil maps may help to better identify a and V_{soil}. A limitation of the

regional sensitivity analysis approach used here is that parameter interactions are only included implicitly, considering parameter interactions with more elaborate methods (Saltelli et al., 2008) may reveal even more characteristics of the VarKarst-R model at different simulation time scales. But this is beyond the scope of this paper.

4.3 Impact of karstic subsurface heterogeneity

Even though some deviations occur among the individual karst landscapes, the general simulations of the VarKarst-R model follow well the observations of mean annual recharge rates over Europe and the Mediterranean (Figure 9). On the other hand, the widely-used large-scale simulation models PCR-GLOBWB (Wada et al., 2010, 2014) and WaterGAP (Döll and Fiedler, 2008b; Döll et al., 2003) generally under-estimate groundwater recharge (Table 6). The reason for this is the representation of karstic subsurface heterogeneity within the VarKarst-R model, i.e. the inclusion of preferential flowpaths and of subsurface heterogeneity. Based on the conceptual understanding of soil and epikarst storage behaviour (Figure 1c) it allows (1) for more recharge during wet conditions because surface runoff is not generated, and (2) for more recharge during dry conditions because the thin soil compartments will always allow for some water to percolate downwards before it is consumed by evapotranspiration. During wet conditions, both PCR-GLOBWB and WaterGAP would produce surface runoff instead that is subsequently lost from groundwater recharge. During dry conditions, due to its non-variable soil storage capacity, the PCR-GLOBWB model would not produce any recharge when the soil water is below its minimum storage. Separating surface runoff and groundwater recharge by a constant factor the WaterGAP model would produce recharge during dry conditions, but a constant fraction of effective precipitation will always become fast surface/subsurface runoff resulting in reduced recharge volumes.

This does not mean that the representation of recharge processes in models like PCR-GLOBWB or WaterGAP is generally wrong, but can be limited since our analysis shows that the structures of such models need more adaption to the particularities of different hydrologic landscapes. In particular it adds to the need for incorporating sub-grid heterogeneity in our large-scale simulation models (Beven and Cloke, 2012). Karst regions comprise about 35% of Europe's land surface and our results indicate that presently their groundwater recharge is under-estimated, while surface runoff and actual evaporation are over-estimated. Given the expected decrease of precipitation in semi-arid regions, such as the Mediterranean, and an

increase of extreme rainfall events at the same time in the near future (2016-2035, Kirtman et al., 2013) current large-scale simulation models will over-estimate both the vulnerability of groundwater recharge and the flood hazard in karst regions in Europe and the Mediterranean. The same is true for the long-term future (end of 21st century, Collins et al., 2013). Of course, an over-estimation of vulnerability and hazard might be the "lesser evil" compared to an over-estimation. But at times of limited financial resources excessive investments in ensuring the security of drinking water supply and flood risk management for potential future changes may unnecessarily aggravate the socio-economic impacts of climate change.

5 Conclusions

In this study we have presented the first attempt to model groundwater recharge over all karst regions in Europe and the Mediterranean. The model application was made possible by a novel parameter confinement strategy that utilized a combination of *a priori* information and recharge related observations on 4 typical karst landscapes that were identified through cluster analysis. Handling the remaining uncertainty explicitly as *posterior* parameter distributions resulting from the confinement strategy we were finally able to produce recharge simulations and an estimate of their uncertainty. We found an adequate agreement with our new model when comparing our results with independent observations of recharge at study sites over Europe and the Mediterranean. We further show that current large-scale modelling approaches tend to significantly under-estimate recharge volumes.

Overall, our analysis showed that the subsurface heterogeneity of karst regions and the presence of preferential flowpaths enhances recharge. It results in high infiltration capacities prohibiting surface runoff and reducing actual evapotranspiration during wet conditions. On the other hand it allows for recharge during dry conditions because some water can always percolate downwards passing the thin fraction of the distributed soil depths. This particular behaviour suggests that karstic regions might be more resilient to climate change in terms of both flooding and droughts. Drinking water and flood risk management is liable to be based on erroneous information at least at the 35% of Europe's land surface since this is not considered in current large-scale modelling approaches.

However, using recharge directly as a proxy for "available" groundwater resources may not be good in all cases, neither in karst regions nor in other types of aquifers (Bredehoeft, 2002). To precisely estimate the sustainably usable fraction of groundwater the aquifer outflow should be known rather than just the inflow. Further pumpingstrategies should consider the

geometry and transmissivity of the aquifer. Hence, recharge estimation can be considered only as a first proxy of available groundwater and future studies should focus on the large-scale simulation of karst groundwater flow and storage to further improve water resources predictions in karst regions.

Acknowledgements

We want to thank Juergen Strub, research associate at the Chair of Hydrology, Freiburg, Germany, for designing some of the figures and Thomas Godman for collecting references to independent recharge studies. This work was supported by a fellowship within the Postdoc Programme of the German Academic Exchange Service [Andreas Hartmann, DAAD] and by the UK Natural Environment Research Council [Francesca Pianosi, CREDIBLE Project; grant number NE/J017450/1]. The sensitivity analysis was carried out by the SAFE Toolbox (http://bristol.ac.uk/cabot/resources/safe-toolbox/). We thank Petra Döll for providing the mean annual recharge volumes of WaterGAP, and Fanny Sarazin for checking the results of the regional sensitivity analysis.

References

Allocca, V., Manna, F. and De Vita, P.: Estimating annual groundwater recharge coefficient for karst aquifers of the southern Apennines (Italy), Hydrol. Earth Syst. Sci., 18(2), 803–817, doi:10.5194/hess-18-803-2014, 2014.

Andreo, B., Vías, J., Durán, J., Jiménez, P., López-Geta, J. and Carrasco, F.: Methodology for groundwater recharge assessment in carbonate aquifers: application to pilot sites in southern Spain, Hydrogeol. J., 16(5), 911–925 [online] Available from: http://dx.doi.org/10.1007/s10040-008-0274-5, 2008.

Aquilina, L., Ladouche, B. and Doerfliger, N.: Water storage and transfer in the epikarst of karstic systems during high flow periods, J. Hydrol., 327, 472–485, 2006.

Arnell, N. W.: Relative effects of multi-decadal climatic variability and changes in the mean and variability of climate due to global warming : future streamflows in Britain, J. Hydrol., 270, 195–213, 2003.

Aydin, H., Ekmekci, M. and Soylu, M. E.: Characterization and conceptualization of a relict karst aquifer (bilecik , turkey) karakterizacija in konceptualizacija reliktnega, Acta carsologica, 42(1), 75–92, 2013.

Bakalowicz, M.: Karst groundwater: a challenge for new resources, Hydrogeol. J., 13, 148–160, 2005.

Bakalowicz, M., El, Æ. M. and El-hajj, A.: Karst groundwater resources in the countries of eastern Mediterranean : the example of Lebanon, Environ. Geol., 54, 597–604, doi:10.1007/s00254-007-0854-z, 2008.

Baldocchi, D., Falge, E., Gu, L., Olson, R., Hollinger, D., Running, S., Anthoni, P., Bernhofer, C., Davis, K., Evans, R., Fuentes, J., Goldstein, A., Katul, G., Law, B., Lee, X., Malhi, Y., Meyers, T., Munger, W., Oechel, W., Paw, K. T., Pilegaard, K., Schmid, H. P., Valentini, R., Verma, S., Vesala, T., Wilson, K. and Wofsy, S.: FLUXNET: A New Tool to Study the Temporal and Spatial Variability of Ecosystem–Scale Carbon Dioxide, Water Vapor, and Energy Flux Densities, Bull. Am. Meteorol. Soc., 82(11), 2415–2434, doi:10.1175/1520-0477(2001)082<2415:fantts>2.3.co;2, 2001.

Barbieri, M., Boschetti, T., Petitta, M. and Tallini, M.: Stable isotope (2H, 18O and 87Sr/86Sr) and hydrochemistry monitoring for groundwater hydrodynamics analysis in a karst aquifer (Gran Sasso, Central Italy), Appl. Geochemistry, 20(11), 2063–2081, doi:10.1016/j.apgeochem.2005.07.008, 2005.

Beven, K. J. and Cloke, H. L.: Comment on "Hyperresolution global land surface modeling: Meeting a grand challenge for monitoring Earth's terrestrial water" by Eric F. Wood et al., Water Resour. Res., 48(1), W01801, doi:10.1029/2011WR010982, 2012.

Bonacci, O.: Analysis of the maximum discharge of karst springs, Hydrogeol. J., 9(4), 328–338, doi:10.1007/s100400100142, 2001.

Bredehoeft, J. D.: The water budget myth revisited: why hydrogeologists model, Ground Water, 40(4), 340–345, 2002.

Budyko, D. H. and Miller, M. I.: Climate and life, Academic press, New York., 1974.

Butscher, C. and Huggenberger, P.: Intrinsic vulnerability assessment in karst areas: A numerical modeling approach, Water Resour. Res., 44, W03408, doi:10.1029/2007WR006277, 2008.

Christensen, J. H., Hewitson, B., Busuioc, A., Chen, A., Gao, X., Held, I., Jones, R., Kolli, R. K., Kwon, W.-T., Laprise, R., Rueda, V. M., Mearns, L., Menéndez, C. G., Räisänen, J., Rinke, A., Sarr, A. and Whetton, P.: Regional Climate Projections, in Climate Change 2007: The Physical Science Basis. Contribution of Working Group I to the Fourth Assessment Report of the Intergovernmental Panel on Climate Change, edited by S. Solomon, D. Qin, M. Manning, Z. Chen, M. Marquis, K. B. Averyt, M. Tignor, and H. L. Miller, p. 996, Cambridge University Press, Cambridge, United Kingdom and New York, NY, USA. [online] Available from: http://www.ipcc.ch/publications_and_data/publications_ipcc_fourth_assessment_report_wg1_report_the_physical_science_basis.htm, 2007.

Collins, M., Knutti, R., Arblaster, J. M., Dufresne, J.-L., Fichefet, T., Friedlingstein, P., Gao, X., Gutowski, W. J., Johns, T. and Krinner, G.: Long-term climate change: projections, commitments and irreversibility, in Climate Change 2013: The Physical Science Basis. Contribution of Working Group I to the Fifth Assessment Report of the Intergovernmental Panel on Climate Change, edited by T. F. Stocker, D. Qin, G.-K. Plattner, M. Tignor, S. K.

637 Allen, J. Boschung, A. Nauels, Y. Xia, V. Bex, and P. M. Midgley, pp. 1029–1136,
638 Cambridge University Press, Cambridge, United Kingdom and New York, NY, USA., 2013.

639 COST: COST 65: Hydrogeological aspects of groundwater protection in karstic areas, Final
640 report (COST action 65), edited by D.-G. X. I. I. S. European Comission Research and
641 Development, Eur. Comm. Dir. XII Sci. Res. Dev., Report EUR, 446, 1995.

642 Dai, A.: Increasing drought under global warming in observations and models, Nat. Clim.
643 Chang., 3(1), 52–58, doi:10.1038/nclimate1633, 2012.

644 Döll, P. and Fiedler, K.: Global-scale modeling of groundwater recharge, Hydrol. Earth Syst.
645 Sci., 12(3), 863–885, doi:10.5194/hess-12-863-2008, 2008a.

646 Döll, P. and Fiedler, K.: Global-scale modeling of groundwater recharge, Hydrol. Earth Syst.
647 Sci., 12(3), 863–885, doi:10.5194/hess-12-863-2008, 2008b.

648 Döll, P., Kaspar, F. and Lehner, B.: A global hydrological model for deriving water
649 availability indicators: model tuning and validation, J. Hydrol., 270(1-2), 105–134,
650 doi:10.1016/S0022-1694(02)00283-4, 2003.

651 Dorigo, W. A., Wagner, W., Hohensinn, R., Hahn, S., Paulik, C., Xaver, A., Gruber, A.,
652 Drusch, M., Mecklenburg, S., van Oevelen, P., Robock, A. and Jackson, T.: The International
653 Soil Moisture Network: a data hosting facility for global in situ soil moisture measurements,
654 Hydrol. Earth Syst. Sci., 15(5), 1675–1698, doi:10.5194/hess-15-1675-2011, 2011.

655 Doummar, J., Sauter, M. and Geyer, T.: Simulation of flow processes in a large scale karst
656 system with an integrated catchment model (Mike She) – Identification of relevant parameters
657 influencing spring discharge, J. Hydrol., 426-427, 112–123,
658 doi:10.1016/j.jhydrol.2012.01.021, 2012.

659 Einsiedl, F.: Flow system dynamics and water storage of a fissured-porous karst aquifer
660 characterized by artificial and environmental tracers, J. Hydrol., 312, 312–321, 2005.

661 Ek, M. B.: Implementation of Noah land surface model advances in the National Centers for
662 Environmental Prediction operational mesoscale Eta model, J. Geophys. Res., 108(D22),
663 doi:10.1029/2002jd003296, 2003.

664 FAO/IIASA/ISRIC/ISSCAS/JRCv: Harmonized World Soil Database (version 1.2), edited by
665 FAO/IIASA, 2012.

666 Fleury, P., Plagnes, V. and Bakalowicz, M.: Modelling of the functioning of karst aquifers
667 with a reservoir model: Application to Fontaine de Vaucluse (South of France), J. Hydrol.,
668 345, 38–49, 2007.

669 Ford, D. C. and Williams, P. W.: Karst Hydrogeology and Geomorphology, Wiley,
670 Chichester., 2007.

671 Foster, S. S. D.: Groundwater recharge and pollution vulnerability of British aquifers: a
672 critical overview, Geol. Soc. London, Spec. Publ., 130, 7–22,
673 doi:10.1144/GSL.SP.1998.130.01.02, 1998.

674 Gleeson, T., Moosdorf, N., Hartmann, J. and van Beek, L. P. H.: A glimpse beneath earth's
675 surface: GLobal HYdrogeology MaPS (GLHYMPS) of permeability and porosity, Geophys.
676 Res. Lett., n/a–n/a, doi:10.1002/2014gl059856, 2014a.

677 Gleeson, T., Moosdorf, N., Hartmann, J. and van Beek, L. P. H.: A glimpse beneath earth's
678 surface: GLobal HYdrogeology MaPS (GLHYMPS) of permeability and porosity, Geophys.
679 Res. Lett., 41(11), 3891–3898, doi:10.1002/2014GL059856, 2014b.

680 Gleeson, T., Wada, Y., Bierkens, M. F. and van Beek, L. P.: Water balance of global aquifers
681 revealed by groundwater footprint, Nature, 488(7410), 197–200, doi:10.1038/nature11295,
682 2012.

683 Goldreich, Y.: The climate of Israel: observation, research and application, Kluwer
684 Academic/Plenum Publishers., 2003.

685 GRDC: Long Term Mean Annual Freshwater Surface Water Fluxes into the World Oceans,
686 Comparisons of GRDC freshwater flux estimate with literature. [online] Available from:
687 http://grdc.bafg.de/servlet/is/7083/, 2004.

688 Hartmann, A., Barberá, J. A., Lange, J., Andreo, B. and Weiler, M.: Progress in the
689 hydrologic simulation of time variant recharge areas of karst systems – Exemplified at a karst
690 spring in Southern Spain, Adv. Water Resour., 54, 149–160,
691 doi:10.1016/j.advwatres.2013.01.010, 2013a.

692 Hartmann, A., Goldscheider, N., Wagener, T., Lange, J. and Weiler, M.: Karst water
693 resources in a changing world: Review of hydrological modeling approaches, Rev. Geophys.,
694 DOI: 10.1002/2013rg000443, doi:10.1002/2013rg000443, 2014a.

695 Hartmann, A., Kobler, J., Kralik, M., Dirnböck, T., Humer, F. and Weiler, M.: Transit time
696 distributions to understand the biogeochemical impacts of storm Kyrill on an Austrian karst
697 system, Biogeosciences, submitted, 2015.

698 Hartmann, A., Lange, J., Weiler, M., Arbel, Y. and Greenbaum, N.: A new approach to model
699 the spatial and temporal variability of recharge to karst aquifers, Hydrol. Earth Syst. Sci.,
700 16(7), 2219–2231, doi:10.5194/hess-16-2219-2012, 2012.

701 Hartmann, A., Mudarra, M., Andreo, B., Marin, A., Wagener, T. and Lange, J.: Modeling
702 spatio-temporal impacts of hydro-climatic extremes on a karst aquifer in Southern Spain,
703 Water Resour. Res., moderate revisions, resubmit until July 2014,
704 doi:10.1002/2014WR015685, 2014b.

705 Hartmann, A., Mudarra, M., Andreo, B., Marín, A., Wagener, T. and Lange, J.: Modeling
706 spatiotemporal impacts of hydroclimatic extremes on groundwater recharge at a
707 Mediterranean karst aquifer, Water Resour. Res., n/a–n/a, doi:10.1002/2014WR015685,
708 2014c.

709 Hartmann, A., Weiler, M., Wagener, T., Lange, J., Kralik, M., Humer, F., Mizyed, N.,
710 Rimmer, A., Barberá, J. A., Andreo, B., Butscher, C. and Huggenberger, P.: Process-based
711 karst modelling to relate hydrodynamic and hydrochemical characteristics to system
712 properties, Hydrol. Earth Syst. Sci., 17(8), 3305–3321, doi:10.5194/hess-17-3305-2013,
713 2013b.

714 Hatipoglu-Bagci, Z. and Sazan, M. S.: Characteristics of karst springs in Aydıncık (Mersin ,
715 Turkey), based on recession curves and hydrochemical and isotopic parameters, Q. J. Eng.
716 Geol. Hydrogeol., 47(1), 89–99, 2014.

717 Heilman, J. L., Litvak, M. E., McInnes, K. J., Kjelgaard, J. F., Kamps, R. H. and Schwinning,
718 S.: Water-storage capacity controls energy partitioning and water use in karst ecosystems on
719 the Edwards Plateau, Texas, Ecohydrology, 7(1), 127–138, doi:10.1002/eco.1327, 2014.

720 Hirabayashi, Y., Mahendran, R., Koirala, S., Konoshima, L., Yamazaki, D., Watanabe, S.,
721 Kim, H. and Kanae, S.: Global flood risk under climate change, Nat. Clim. Chang., 3(9), 816–
722 821, doi:10.1038/nclimate1911, 2013.

723 Hoetzl, H.: Groundwater recharge in an arid karst area (Saudi Arabia), IAHS Publ.
724 (International Assoc. Hydrol. Sci., 232, 195–207, 1995.

725 Hughes, A. G., Mansour, M. M. and Robins, N. S.: Evaluation of distributed recharge in an
726 upland semi-arid karst system: the West Bank Mountain Aquifer, Middle East, Hydrogeol. J.,
727 16, 845–854, 2008.

728 Jackson, C. R., Meister, R. and Prudhomme, C.: Modelling the effects of climate change and
729 its uncertainty on UK Chalk groundwater resources from an ensemble of global climate
730 model projections, J. Hydrol., In Press, doi:10.1016/j.jhydrol.2010.12.028, 2010.

731 Jeannin, P.-Y. and Grasso, D. A.: Permeability and hydrodynamic behavior of karstic
732 environment, in Karst Waters Environmental Impact, edited by G. Gunay and A. I. Johnson,
733 pp. 335–342, A.A. Balkema, Roterdam., 1997.

734 Jukic, D. and Denic-Jukic, V.: Estimating parameters of groundwater recharge model in
735 frequency domain: Karst springs Jadro and Žrnovnica, Hydrol. Process., 22, 4532–4542,
736 2008.

737 Ketchen, D. J. and Shook, C. L.: The application of cluster analysis, Strateg. Manag. J.,
738 17(November 1994), 441–458, 1996.

739 Kiraly, L.: Modelling karst aquifers by the combined discrete channel and continuum
740 approach, Bull. d'Hydrogéologie, 16, 77–98, 1998.

741 Kiraly, L.: Karstification and Groundwater Flow, Speleogenes. Evol. Karst Aquifers, 1(3), 1–
742 24, 2003.

743 Kirtman, B., Power, S. B., Adedoyin, J. A., Boer, G. J., Bojariu, R., Camilloni, I., Doblas-
744 Reyes, F. J., Fiore, A. M., Kimoto, M. and Meehl, G. A.: Near-term climate change:
745 projections and predictability, in Climate Change 2013: The Physical Science Basis.

746 Contribution of Working Group I to the Fifth Assessment Report of the Intergovernmental
747 Panel on Climate Change, edited by T. F. Stocker, D. Qin, G.-K. Plattner, M. Tignor, S. K.
748 Allen, J. Boschung, A. Nauels, Y. Xia, V. Bex, and P. M. Midgley, pp. 953–1028, Cambridge
749 University Press, Cambridge, United Kingdom and New York, NY, USA., 2013.

750 Kottek, M., Grieser, J., Beck, C., Rudolf, B. and Rubel, F.: World Map of the Köppen-Geiger
751 climate classification updated, Meteorol. Zeitschrift, 15(3), 259–263, doi:10.1127/0941-
752 2948/2006/0130, 2006.

753 Koutroulis, A. G., Tsanis, I. K., Daliakopoulos, I. N. and Jacob, D.: Impact of climate change
754 on water resources status: A case study for Crete Island, Greece, J. Hydrol., 479, 146–158,
755 doi:10.1016/j.jhydrol.2012.11.055, 2013.

756 Lange, J., Greenbaum, N., Husary, S., Ghanem, M., Leibundgut, C. and Schick, A. P.: Runoff
757 generation from successive simulated rainfalls on a rocky, semi-arid, Mediterranean hillslope,
758 Hydrol. Process., 17(2), 279–296, doi:10.1002/hyp.1124, 2003.

759 Lee, E. S. and Krothe, N. C.: A four-component mixing model for water in a karst terrain in
760 south-central Indiana, USA. Using solute concentration and stable isotopes as tracers, Chem.
761 Geol., 179, 2001.

762 Leibowitz, S. G., Comeleo, R. L., Wigington Jr., P. J., Weaver, C. P., Morefield, P. E.,
763 Sproles, E. a. and Ebersole, J. L.: Hydrologic landscape classification evaluates streamflow
764 vulnerability to climate change in Oregon, USA, Hydrol. Earth Syst. Sci., 18(9), 3367–3392,
765 doi:10.5194/hess-18-3367-2014, 2014.

766 Lerner, D. N., Issar, A. S. and Simmers, I.: Groundwater recharge : a guide to understanding
767 and estimating natural recharge, Heise, Hannover., 1990.

768 Lionello, P.: The Climate of the Mediterranean Region: From the past to the future, Elsevier.,
769 2012.

770 Maloszewski, P., Stichler, W., Zuber, A. and Rank, D.: Identifying the flow systems in a
771 karstic-fissured-porous aquifer, the Schneealpe, Austria, by modelling of environmental 18O
772 and 3H isotopes, J. Hydrol., 256, 48–59, 2002.

773 Milly, P. C. D., Dunne, K. A. and Vecchia, A. V: Global pattern of trends in streamflow and
774 water availability in a changing climate, Nature, 438(7066), 347–350,
775 doi:10.1038/nature04312, 2005.

776 Miralles, D. G., Holmes, T. R. H., De Jeu, R. A. M., Gash, J. H., Meesters, A. G. C. A. and
777 Dolman, A. J.: Global land-surface evaporation estimated from satellite-based observations,
778 Hydrol. Earth Syst. Sci., 15(2), 453–469, doi:10.5194/hess-15-453-2011, 2011.

779 Le Moine, N., Andréassian, V. and Mathevet, T.: Confronting surface- and groundwater
780 balances on the La Rochefoucauld-Touvre karstic system (Charente, France), Water Resour.
781 Res., 44, W03403, doi:10.1029/2007WR005984, 2008.

Le Moine, N., Andréassian, V., Perrin, C. and Michel, C.: How can rainfall-runoff models handle intercatchment groundwater flows? Theoretical study based on 1040 French catchments, Water Resour. Res., 43, W06428, doi:10.1029/2006WR005608, 2007.

Mudarra, M. and Andreo, B.: Relative importance of the saturated and the unsaturated zones in the hydrogeological functioning of karst aquifers: The case of Alta Cadena (Southern Spain), J. Hydrol., 397(3-4), 263–280, doi:10.1016/j.jhydrol.2010.12.005, 2011.

Padilla, A., Pulido-Bosch, A. and Mangin, A.: Relative Importance of Baseflow and Quickflow from Hydrographs of Karst Spring, Ground Water, 32(2), 267–277, 1994.

Perrin, J., Jeannin, P.-Y. and Zwahlen, F.: Epikarst storage in a karst aquifer: a conceptual model based on isotopic data, Milandre test site, Switzerland, J. Hydrol., 279, 106–124, 2003.

Priestley, C. H. B. and Taylor, R. J.: On the Assessment of Surface Heat Flux and Evaporation Using Large-Scale Parameters, Mon. Weather Rev., 100(2), 81–92, doi:10.1175/1520-0493(1972)100<0081:OTAOSH>2.3.CO;2, 1972.

Quinn, J. J., Tomasko, D. and Kuiper, J. A.: Modeling complex flow in a karst aquifer, Sediment. Geol., 184, 343–352, 2006.

Rimmer, A. and Hartmann, A.: Simplified conceptual structures and analytical solutions for groundwater discharge using reservoir equations, Water Resour. Manag. Model. Ed. by DPC Nayak, InTech, Kakinada, India, 217–338, 2012.

Rodell, M., Houser, P. R., Jambor, U., Gottschalck, J., Mitchell, K., Meng, C.-J., Arsenault, K., Cosgrove, B., Radakovich, J., Bosilovich, M., Entin, J. K., Walker, J. P., Lohmann, D. and Toll, D.: The Global Land Data Assimilation System, Bull. Am. Meteorol. Soc., 85(3), 381–394, doi:10.1175/BAMS-85-3-381, 2004.

Rui, H. and Beaudoing, H.: README Document for Global Land Data Assimilation System Version 2 (GLDAS-2) Products, GES DISC / HSL [online] Available from: http://hydro1.sci.gsfc.nasa.gov/data/s4pa/GLDAS/README.GLDAS2.pdf, 2013.

Saltelli, A., Ratto, M., Andres, T., Campolongo, F., Cariboni, J., Gatelli, D., Saisana, M. and Tarantola, S.: Global sensitivity analysis: the primer, John Wiley & Sons., 2008.

Samuels, R., Rimmer, A., Hartmann, A., Krichak, S. and Alpert, P.: Climate Change Impacts on Jordan River Flow: Downscaling Application from a Regional Climate Model, J. Hydrometeorol., 11(4), 860–879, doi:DOI 10.1175/2010JHM1177.1, 2010.

Sawicz, K., Wagener, T., Sivapalan, M., Troch, P. A. and Carrillo, G.: Catchment classification: empirical analysis of hydrologic similarity based on catchment function in the eastern USA, Hydrol. Earth Syst. Sci., 15(9), 2895–2911, doi:10.5194/hess-15-2895-2011, 2011.

Scanlon, B., Healy, R. and Cook, P.: Choosing appropriate techniques for quantifying groundwater recharge, Hydrogeol. J., 10(1), 18–39 [online] Available from: http://dx.doi.org/10.1007/s10040-001-0176-2, 2002.

819 Seber, G. A. F.: Multivariate observations, John Wiley & Sons., 2009.

820 Sivapalan, M., Yaeger, M. a., Harman, C. J., Xu, X. and Troch, P. a.: Functional model of
821 water balance variability at the catchment scale: 1. Evidence of hydrologic similarity and
822 space-time symmetry, Water Resour. Res., 47(2), W02522, doi:10.1029/2010WR009568,
823 2011.

824 Spear, R. C. and Hornberger, G. M.: Eutriphication in peel inlet - II. Identification of critical
825 uncertainties via generalized sensitivity analysis, Water Resour. Res., 14, 43–49, 1980.

826 Tague, C. and Grant, G. E.: Groundwater dynamics mediate low-flow response to global
827 warming in snow-dominated alpine regions, Water Resour. Res., 45(7), W07421,
828 doi:10.1029/2008WR007179, 2009.

829 Tritz, S., Guinot, V. and Jourde, H.: Modelling the behaviour of a karst system catchment
830 using non-linear hysteretic conceptual model, J. Hydrol., 397(3-4), 250–262,
831 doi:10.1016/j.jhydrol.2010.12.001, 2011.

832 USGS: Shuttle Radar Topography Mission, 3 Arc Second scene SRTM V2.1, edited by U. of
833 M. Global Land Cover Facility, 2006.

834 Vaute, L., Drogue, C., Garrelly, L. and Ghelfenstein, M.: Relations between the structure of
835 storage and the transport of chemical compounds in karstic aquifers, J. Hydrol., 199, 221–
836 238, 1997.

837 Vita, P. De, Allocca, V., Manna, F. and Fabbrocino, S.: Coupled decadal variability of the
838 North Atlantic Oscillation , regional rainfall and karst spring discharges in the Campania
839 region (southern Italy), , 1389–1399, doi:10.5194/hess-16-1389-2012, 2012.

840 Viviroli, D., Dürr, H. H., Messerli, B., Meybeck, M. and Weingartner, R.: Mountains of the
841 world, water towers for humanity: Typology, mapping, and global significance, Water
842 Resour. Res., 43(7), W07447, doi:10.1029/2006WR005653, 2007.

843 De Vries, J. J. and Simmers, I.: Groundwater recharge: an overview of processes and
844 challenges, Hydrogeol. J., 10(1), 5–17, doi:10.1007/s10040-001-0171-7, 2002.

845 Wada, Y., van Beek, L. P. H., van Kempen, C. M., Reckman, J. W. T. M., Vasak, S. and
846 Bierkens, M. F. P.: Global depletion of groundwater resources, Geophys. Res. Lett., 37(20),
847 L20402, doi:10.1029/2010gl044571, 2010.

848 Wada, Y., Wisser, D. and Bierkens, M. F. P.: Global modeling of withdrawal, allocation and
849 consumptive use of surface water and groundwater resources, Earth Syst. Dyn., 5(1), 15–40,
850 doi:10.5194/esd-5-15-2014, 2014.

851 Wagener, T., Sivapalan, M., Troch, P. A., McGlynn, B. L., Harman, C. J., Gupta, H. V,
852 Kumar, P., Rao, P. S. C., Basu, N. B. and Wilson, J. S.: The future of hydrology: An evolving
853 science for a changing world, Water Resour. Res., 46(5), W05301,
854 doi:10.1029/2009wr008906, 2010.

Wellings, S. R.: Recharge of the Upper Chalk aquifer at a site in Hampshire, England, J. Hydrol., 69, 275–285, doi:10.1016/0022-1694(84)90167-7, 1984.

Wigington, P. J., Leibowitz, S. G., Comeleo, R. L. and Ebersole, J. L.: OREGON HYDROLOGIC LANDSCAPES : A CLASSIFICATION FRAMEWORK 1, J. Am. Water Resour. Assoc., 49(1), 163–182, doi:10.1111/jawr.12009, 2013.

Williams, P. W.: The role of the Subcutaneous zone in karst hydrology, J. Hydrol., 61, 45–67, 1983.

Williams, P. W. and Ford, D. C.: Global distribution of carbonate rocks, Zeitschrift für Geomorphol., Suppl. 147, 1–2, 2006.

Winter, T. C.: The Concept of Hydrologic Landscapes, JAWRA J. Am. Water Resour. Assoc., 37(2), 335–349, doi:10.1111/j.1752-1688.2001.tb00973.x, 2001.

Wood, E. F., Roundy, J. K., Troy, T. J., van Beek, L. P. H., Bierkens, M. F. P., Blyth, E., de Roo, A., Döll, P., Ek, M., Famiglietti, J., Gochis, D., van de Giesen, N., Houser, P., Jaffé, P. R., Kollet, S., Lehner, B., Lettenmaier, D. P., Peters-Lidard, C., Sivapalan, M., Sheffield, J., Wade, A. and Whitehead, P.: Hyperresolution global land surface modeling: Meeting a grand challenge for monitoring Earth's terrestrial water, Water Resour. Res., 47(5), W05301, doi:10.1029/2010WR010090, 2011.

Zagana, E., Tserolas, P., Floros, G., Katsanou, K. and Andreo, B.: First outcomes from groundwater recharge estimation in evaporate aquifer in Greece with the use of APLIS method, in Advances in the Research of Aquatic Environment, edited by N. Lambrakis, G. Stournaras, and K. Katsanou, pp. 89–96, Springer Berlin Heidelberg., 2011.

878 # Tables

879 **Table 1: Data availability, data properties and sources**

Variable	Spatial resolution	Time period	Frequency	Source	Reference
Precipitation	0.25°	2002-2012	daily	GLDAS-2	(Rodell et al., 2004; Rui and Beaudoing, 2013)
Temperature	0.25°	2002-2012	daily	GLDAS-2	
Net radiation	0.25°	2002-2012	daily	GLDAS-2	
Snow water equivalent	0.25°	2002-2012	daily	NOAHv3.3 /GLDAS-2	(Ek, 2003; Rodell et al., 2004)
Carbonate rock areas	vector data	-	-		(Williams and Ford, 2006)
Elevation	3''	-	-	SRMT V2.1	(USGS, 2006)
Rock permeability	vector data	-	-		(Gleeson et al., 2014a)
Actual evaporation	individual locations	individual periods	daily	FLUXNET	(Baldocchi et al., 2001)
Soil moisture	Individual locations	individual periods	daily	ISMN	(Dorigo et al., 2011)

880

881 **Table 2: Parameter description and initial ranges for Monte Carlo sampling based on previous field**
882 **studies and large-scale model applications**

Parameter	Unit	Description	Lower Limit*	Upper limit*	References
a	[-]	Variability constant	0	6	(Hartmann et al., 2013b, 2014c, 2015)
V_{soil}	[mm]	Mean soil storage capacity	0	1250	(Miralles et al., 2011; FAO/IIASA/ISRIC/ISSCAS/JRCv, 2012; Ek, 2003)
V_{epi}	[mm]	Mean epikarst storage capacity	200	700	(Perrin et al., 2003; Williams, 2008)
K_{epi}	[d]	Mean epikarst storage coefficient	0	50	(Gleeson et al., 2014b; Hartmann et al., 2013b)

883

884

885

886 **Table 3: Independent observations of mean annual recharge from field and modelling studies over Europe**
887 **and the Mediterranean**

Location	Latitude	Longitude	Mean annual recharge	Method	Author
(country, province)	[dec. degr.]	[dec. degr.]	[mm]		
Austria (Siebenquellen spring, Schneeaple)	47.69	15.6	694	observed water balance	(Maloszewski et al., 2002)
Croatia (Jadro spring, Dugopolje)	43.58	16.6	795	simulated water balance	(Jukic and Denic-Jukic, 2008)
Croatia (St. Ivan, Mirna)	45.22	13.6	386	observed water balance	(Bonacci, 2001)
France (Bonnieure, La Rouchefoucald-Touvre)	45.8	0.44	250	simulated water balance	(Le Moine et al., 2007)
France (Durzon spring, La Cavalerie)	44.01	3.16	378	observed water balance	(Tritz et al., 2011)
France (Fontaine de Vaucluse)	43.92	5.13	568	observed water balance	(Fleury et al., 2007)
France (St Hippolyte-du-Fort, Vidourle)	43.93	3.85	287	observed water balance	(Vaute et al., 1997)
Germany (Bohming spring, Rieshofen)	48.93	11.3	130	observed water balance	(Einsiedl, 2005)
Germany (Gallusquelle spring, Swabian Albs)	48.21	9.15	351	observed water balance	(Doummar et al., 2012)
Germany (Hohenfells)	49.2	11.8	200	observed water balance	(Quinn et al., 2006)
Greece (Arvi, Crete)*	35.13	24.55	241	observed water balance	(Koutroulis et al., 2013)
Greece (Aitoloakarnania)	38.60	21.15	484	empiric estimation method	(Zagana et al., 2011)
Italy (Cerella spring, Latina)	41.88	12.9	416	empiric estimation method	(Allocca et al., 2014)
Italy (Forcella spring, Sapri)	41.05	14.55	559	empiric estimation method	(Allocca et al., 2014)
Italy (Gran Sasso, Teramo)	42.27	13.34	700	observed water balance	(Barbieri et al., 2005)
Italy (Sanità)	40.78	15.13	974	observed water balance	(Vita et al., 2012)
Italy (Taburno spring)	39.9	15.81	693	empiric estimation method	(Allocca et al., 2014)
Lebanon (Anjar-Chamsine)	33.73	35.93	278	observed water balance	(Bakalowicz et al., 2008)
Lebanon (Zarka)	34.08	36.30	205	observed water balance	(Bakalowicz et al., 2008)
Lebanon (Afka)	34.05	35.95	842	observed water balance	(Bakalowicz et al., 2008)
Palestine (Mountain Aquifer)	~32.00	~35.30	144	simulated water balance	(Hughes et al., 2008)
Portugal (Algarve, minimum value)	~37.10	~-7.90	130	not mentioned	(de Vries and Simmers, 2002)
Portugal (Algarve, maximum value)	~37.10	~-7.90	300	not mentioned	(de Vries and Simmers, 2002)
Saudi Arabia (Eastern Arabian peninsula)	~26.50	~46.50	44	natural tracers	(Hoetzl, 1995)
Spain (Cazorla, Sierra de Cazorla)	37.9	-3.03	244	empiric estimation method	(Andreo et al., 2008)
Spain (La Villa spring, El Torcel)	36.93	-4.52	463	observed water balance	(Padilla et al., 1994)
Spain (Sierra de las Cabras, Arcos de la frontera)	36.65	-5.72	318	empiric estimation method	(Andreo et al., 2008)
Switzerland (Rappenfluh Spring)	47.87	7.67	650	simulated water balance	(Butscher and Huggenberger, 2008)
Turkey (Aydincik, Mersin)	36.97	33.22	552	observed water balance	(Hatipoglu-Bagci and Sazan, 2014)
Turkey (Harmankoy, Beyyayla)	40.15	30.65	32	observed water balance	(Aydin et al., 2013)
UK (Marlborough and Berkshire Downs and South-West Chilterns,	51.53	-1.15	146	simulated water balance	(Jackson et al., 2010)

minimum value)					
UK (Marlborough and Berkshire Downs and South-West Chilterns, maximum value)	51.53	-1.15	365	simulated water balance	(Jackson et al., 2010)
UK (Dorset)	50.75	-2.45	700	observed water balance	(Foster, 1998)
UK (Norfolk)	52.60	0.88	260	observed water balance	(Foster, 1998)
UK (Greta spring, Durham)	54.52	-1.87	690	observed water balance	(Arnell, 2003)
UK(R. Teme, Tenbury wells)	52.3	-2.58	355	observed water balance	(Arnell, 2003)
UK(Lambourn)	51.5	-1.53	234	observed water balance	(Arnell, 2003)
UK (Hampshire)	51.1	-1.26	348	observed water balance	(Wellings, 1984)

Table 4: Cluster means of the 4 identified karst landscapes (AI: aridity index, DS mean annual number of days with snow cover, RA: range of altitudes)

descriptor	unit	number of cluster/karst landscape			
		1.HUM	2.MTN	3.MED	4.DES
AI	[-]	0.80	0.98	3.18	20.00
DS	[a-1]	85	76	16	1
RA	[m]	228	1785	691	232

Table 5: Minima and maxima of the confined parameter samples for each of the identified landscapes

Parameter	Unit	HUM		MTN		MED		DES	
		min	max	min	max	min	max	min	max
α	[-]	1.1	3.3	0.3	2.9	0.8	6.0	0.1	6.0
V_{soil}*	[mm]	900.1 (900)	1248.9 (1250)	500.4 (500)	899.9 (900)	51.7 (50)	498.4 (500)	0.2 (0)	49.1 (500)
V_{epi}	[mm]	204.3	694.8	201.6	699.4	200.1	696.7	202.3	695.7
K_{epi}	[d]	0.0	35.8	7.3	49.9	0.0	48.4	10.4	49.9

* in brackets: *a priori* infromation used for step 3 of the parameter confinement strategy

Table 6: Mean deviations of the VarKarst-R, the PCR-GLOBWB model and the WaterGAP model from all observations and the individual regions

region	mean deviation [mm/a]		
	VarKarst-R	PCR-GLOBWB	WaterGAP
all	-58.3	-230.4	-264.2
HUM	65.5	-90.2	-151.6
MTN	-202.8	-427.5	-446.4
MED	-4.3	-217.3	-211.4

Figures

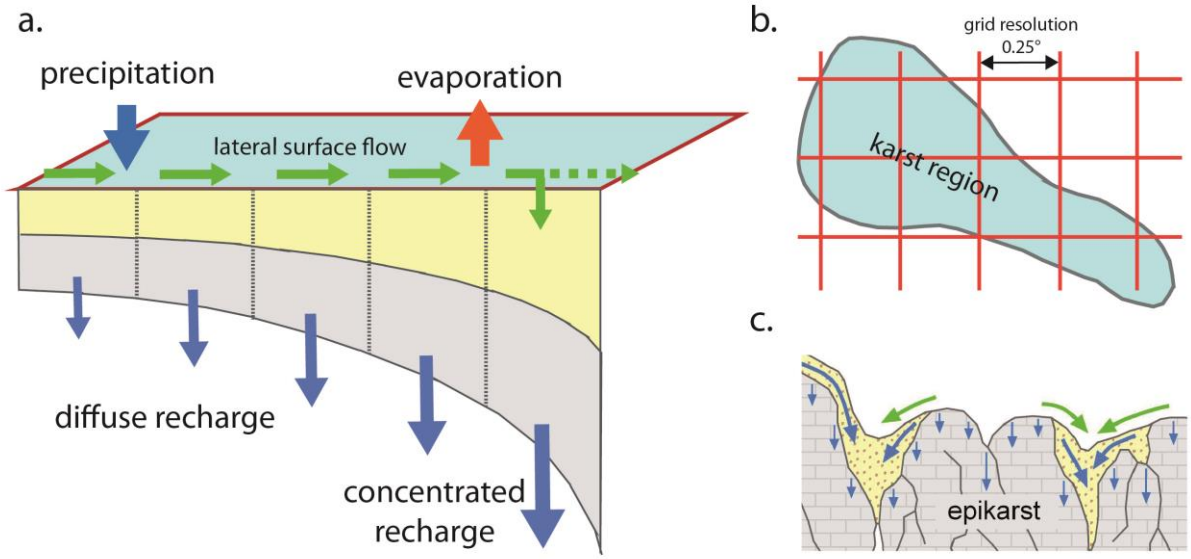

Figure 1: (a) schematic description of the model for one grid cell including the soil (yellow) and epikarst storages (grey) and the simulated fluxes, (b) its gridded discretisation over karst regions and (c) the subsurface heterogeneity that its structure represents for each grid cell.

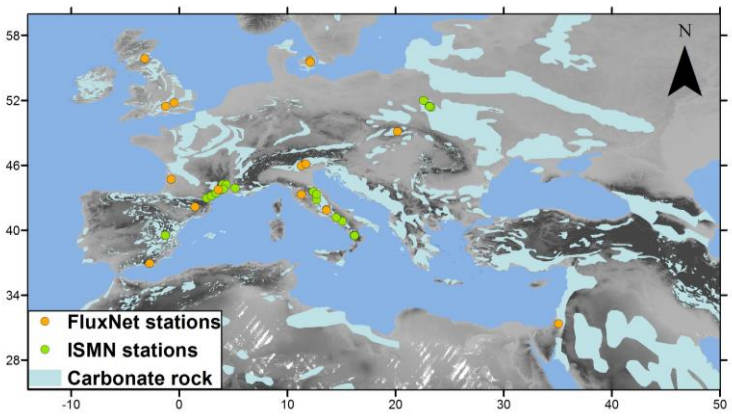

Figure 2: Carbonate rock areas over Europe and the Mediterranean, and location of the selected FLUXNET and ISMN stations

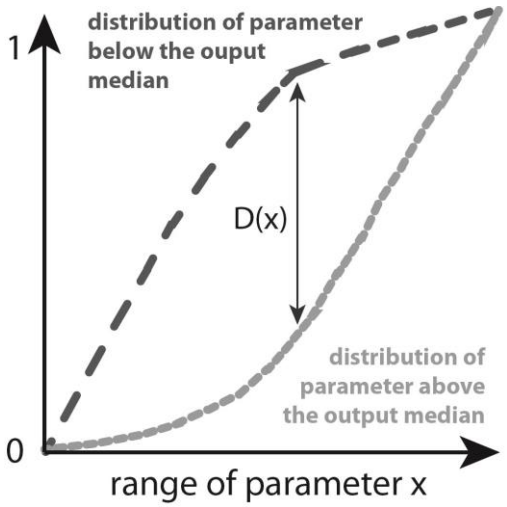

911

912 **Figure 3: Schematic elaboration of the regional sensitivity analysis procedure**

913

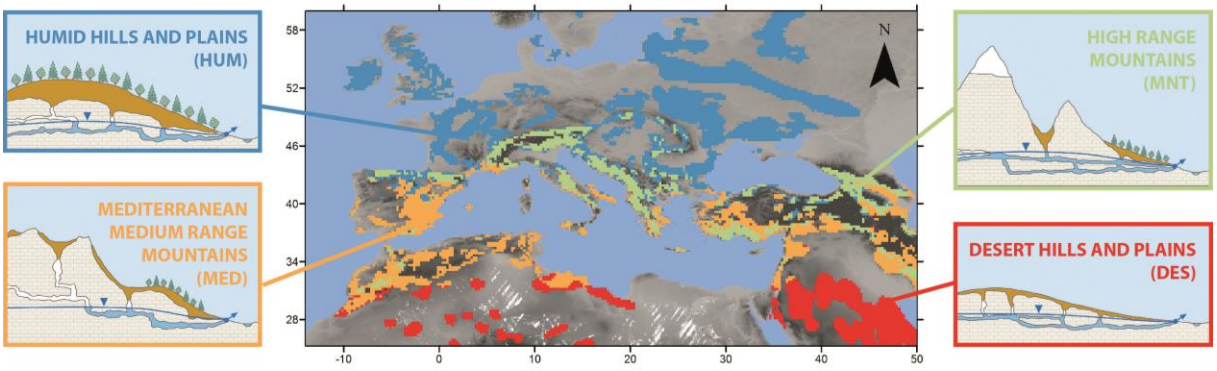

914

915 **Figure 4: Map with clusters and typical karst landscapes that were attributed to them**

916

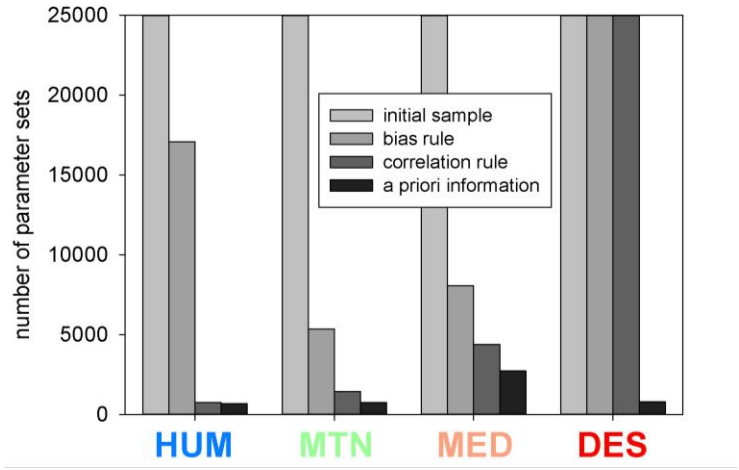

917

918 **Figure 5: Evolution of the initial sample of 25,000 parameter sets (each including the 4 model parameters**
919 **sampled from within their initial ranges) along the different confinement steps for the 4 karst landscapes**

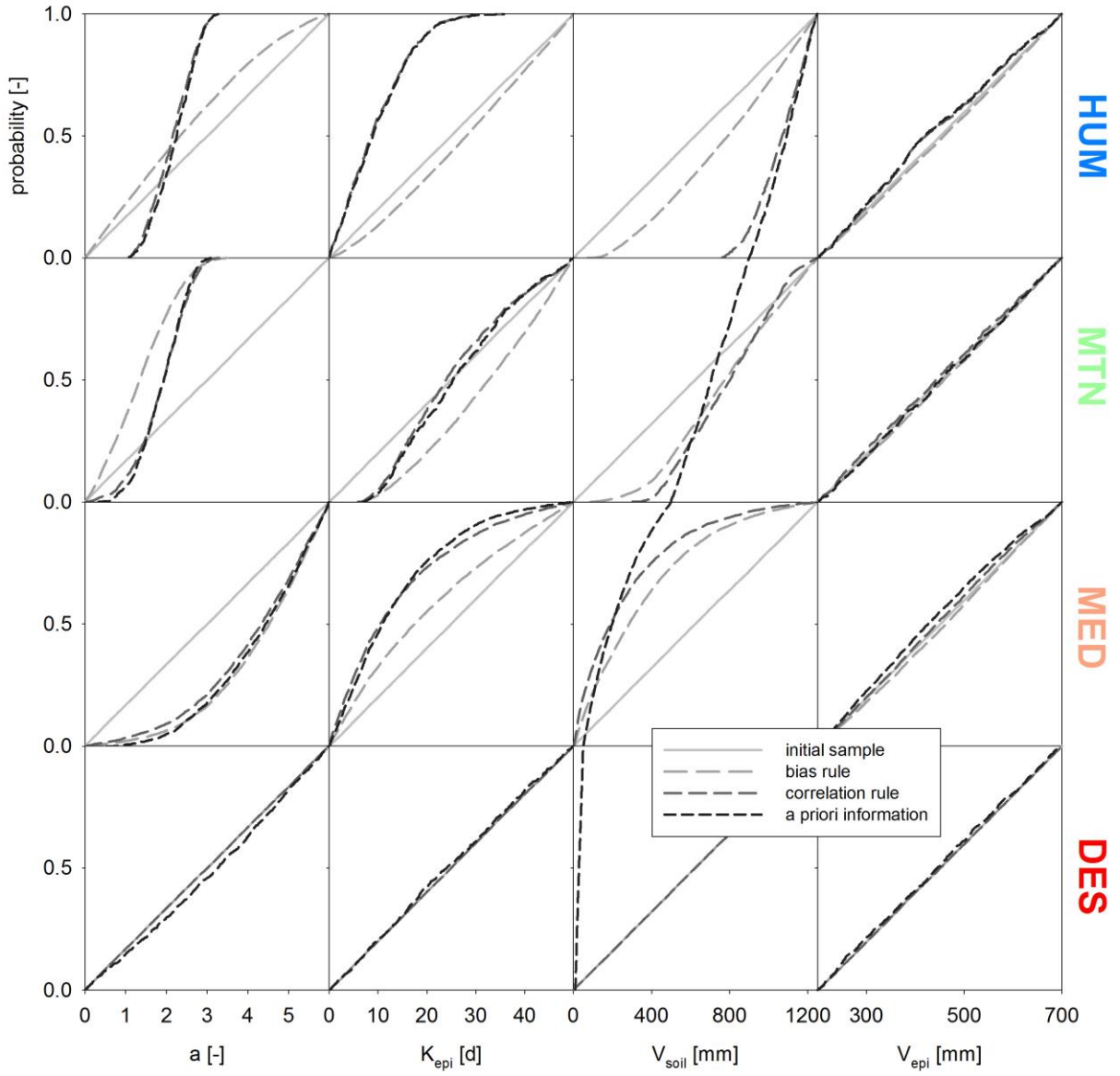

920

921 **Figure 6: Evolution of *posterior* probabilities of the 4 model parameters for the 4 karst landscapes along**
922 **the steps of the parameter confinement strategy.**

923

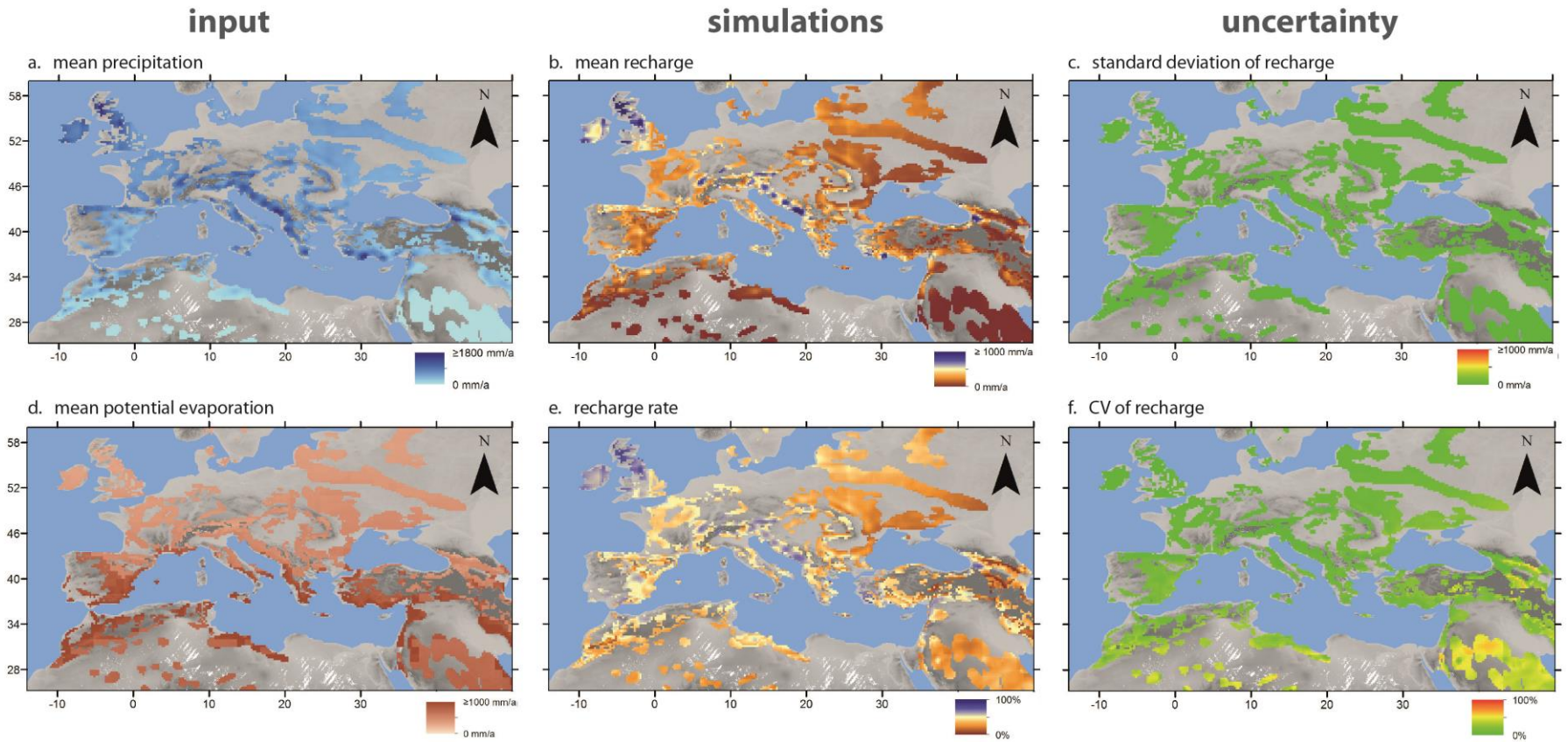

924

925 **Figure 7: (a) Observed precipitation and (d) potential evaporation versus the simulated (b) mean annual recharge and (e) mean annual recharge rates derived**
926 **from the mean of all 250 parameter sets, and (c) the standard deviation and (f) coefficients of variation of the simulations due to the variability among the 250**
927 **parameter sets.**

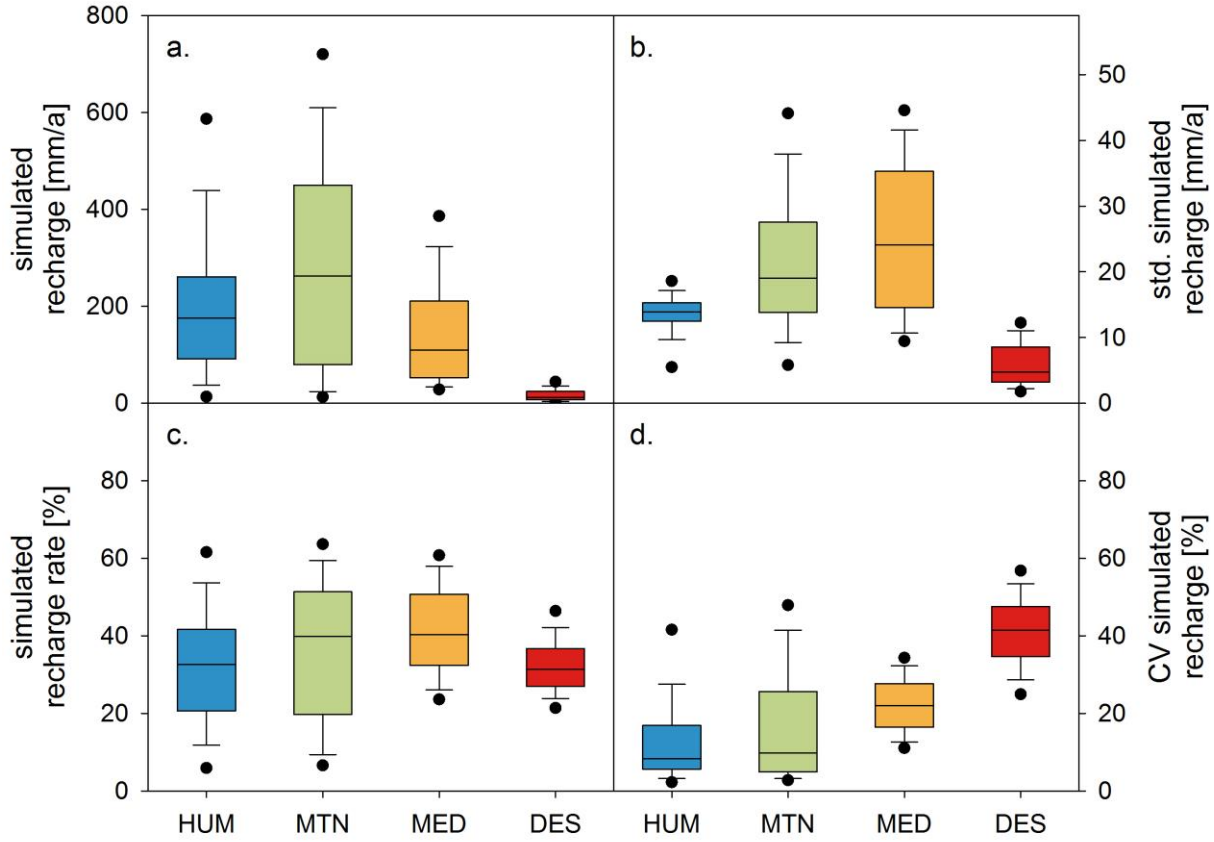

928

929 **Figure 8: (a) Simulated mean annual recharge, among the 4 karst landscapes, (b) their standard**
930 **deviations, (c) recharge rates, and (d) coefficients of variation obtained by the final sample of parameters.**

931

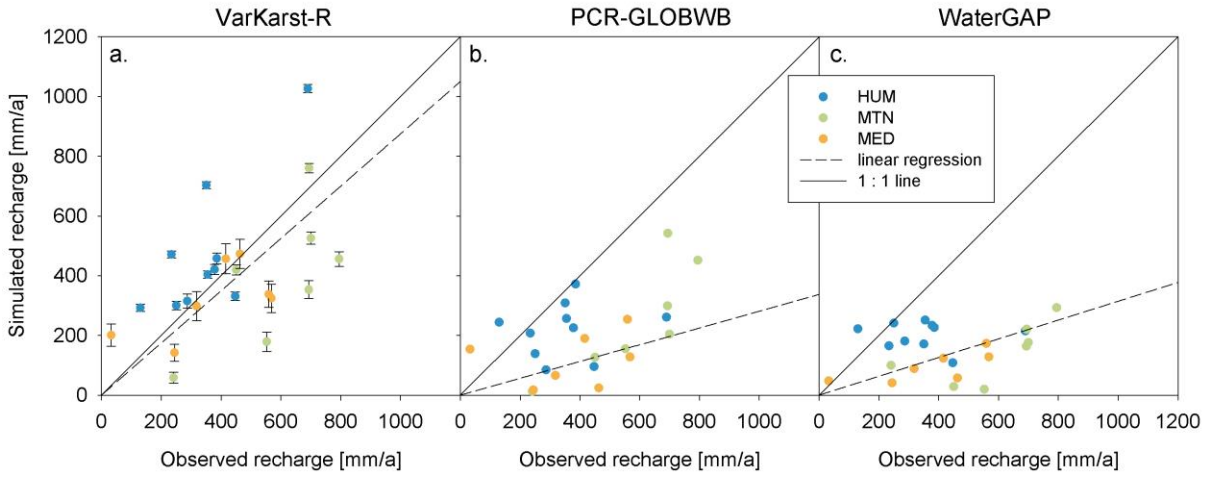

932

933 **Figure 9: Observations of mean annual recharge from independent studies (Table 3) versus the simulated**
934 **mean annual recharge by the VarKarst-R and the PCR-GLOBWB model (no data for the DES region**
935 **available)**

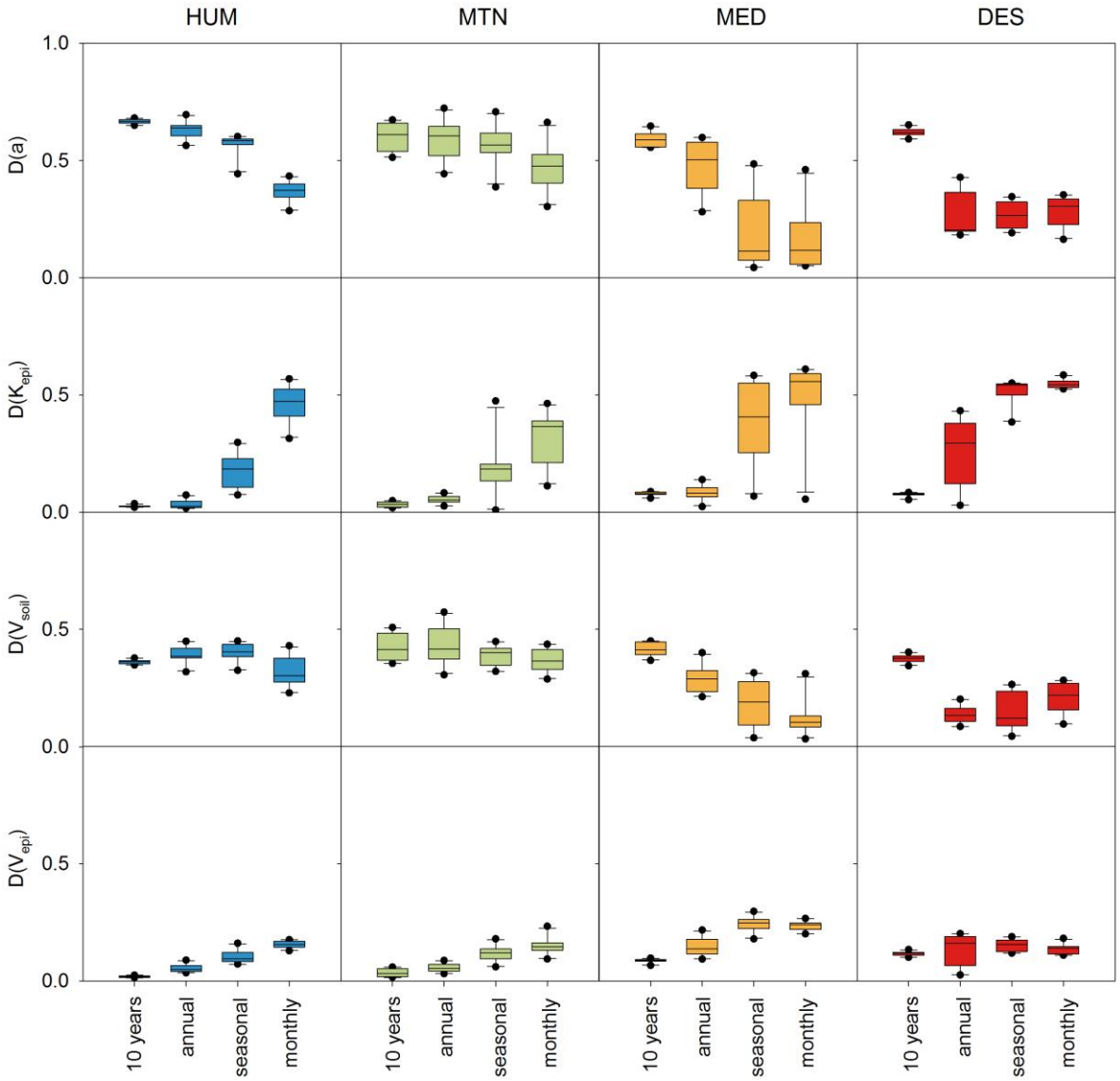

Figure 10: Sensitivity of simulated recharge to the model parameters at different time scales and in the different karst landscapes. Sensitivity is measured by the maximum distance (D) between the distribution of parameter sets that produce 'low' recharge (i.e. below the median) and the distribution producing 'high' recharge (above the median). Parameter sets are initially sampled from the ranges in Table 2.

6 Appendix

6.1 Results of the cluster analysis

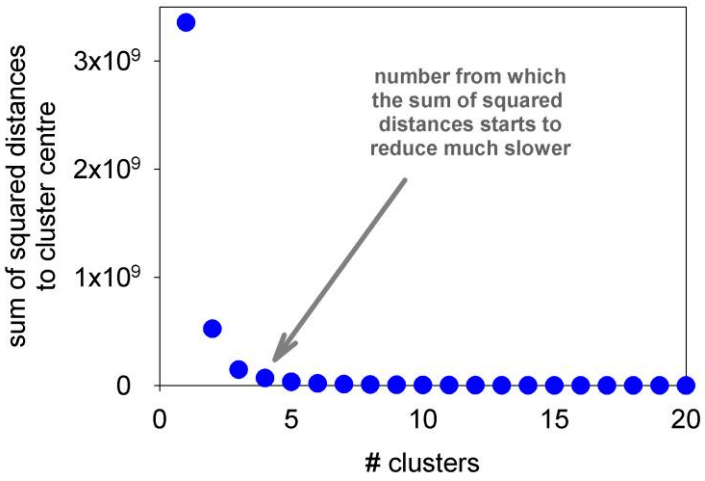

Figure A 1: Elbow plot of sum of squared distances to cluster centres for k-means method

6.2 Results of the regional sensitivity using initial ranges

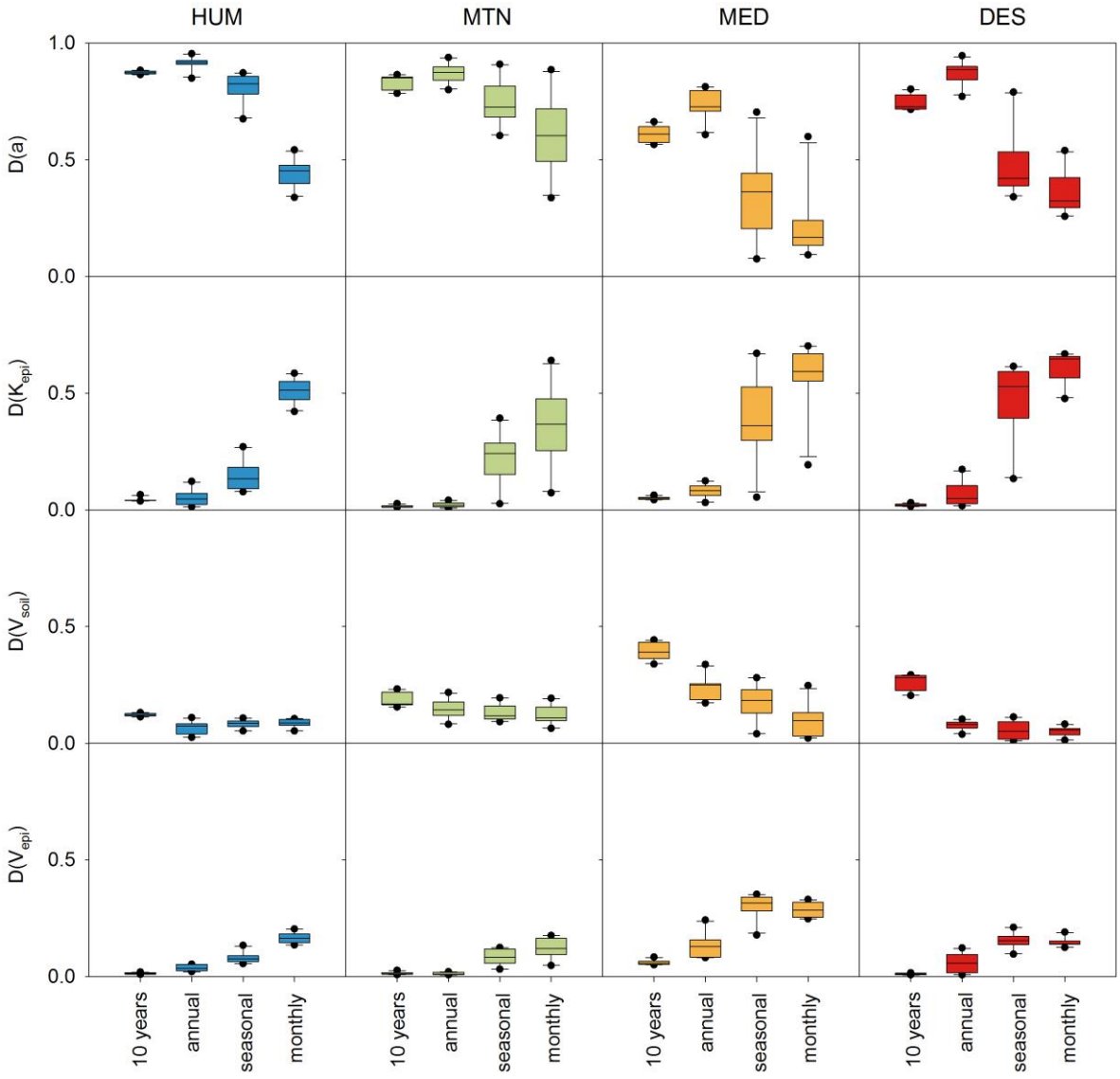

Figure A 2: Sensitivity of simulated recharge to the model parameters at different time scales and in the different karst landscapes, as in Figure 10 but sampling parameters from the confined parameter ranges of Table 5